Data-Based Learning for Control and Prediction of Robot-Structure Interactions with Comparable Robot and Structure Stiffnesses

Lance O. McCann

A dissertation
submitted in partial fulfillment of the
requirements for the degree of

Doctor of Philosophy

University of Washington

2024

Reading Committee:
Santosh Devasia, Chair
Joseph Garbini, Chair
Ramulu Mamidala

Program Authorized to Offer Degree:
Mechanical Engineering

University of Washington

Abstract

Data-Based Learning for Control and Prediction of Robot-Structure Interactions with Comparable Robot and Structure Stiffnesses

Lance O. McCann

Co-Chairs of the Supervisory Committee:
Professor Santosh Devasia
Mechanical Engineering

Professor Joseph Garbini
Mechanical Engineering

Efficient and accurate robotic interactions with flexible structures are critical for many manufacturing processes where the elasticity of the workpiece and the robot must be accounted for. In particular, for clamping and drilling flexible structures, maintaining tool-workpiece normality and limiting shear forces are essential. The main contributions of this thesis are to show: Firstly, that data acquired during a robotic clamping operation can be learned and used to speed up the process for similar operations. Utilizing the learned parameters, a map between the measured forces and robot joint positions is used to develop time-based robot-joint (velocity) trajectories to achieve a specified robot-workpiece interaction. Experimental results show that the operating speed can be increased while maintaining interaction forces and torques within acceptable levels. Secondly, with a minimum number of learned measurement locations controlled interactions such as clamping operations can be efficiently predicted at unmeasured locations. Gaussian Process Regression methods are presented as a suitable means to predict interactions, ultimately resulting in increased interaction speeds at workpiece locations where controlled-interactions have not been conducted. Additionally, to minimize the number of measurement locations, a method is developed using existing

interaction data to optimize measurement location selection by minimizing prediction uncertainty.

TABLE OF CONTENTS

LIST OF FIGURES

LIST OF TABLES

ACKNOWLEDGMENTS

I would like to express my deepest gratitude to my advisors Professor Joseph Garbini and Professor Santosh Devasia, for their unwavering support, guidance, and encouragement throughout my PhD journey. Their expertise and insightful feedback have been invaluable to my research and professional development.

Special thanks go to my colleagues and friends at University of Washington Department of Mechanical Engineering. The collaborative environment and stimulating discussions have greatly enriched my research experience. In particular, I would like to acknowledge Yoshua Gombo, Chia-Ning Lee, Anuj Tiwari, Leon (Liangwu) Yan and Sarmad Hassan for their contributions to research.

I am deeply indebted to my friends and family for their unwavering love, patience, and encouragement. Their faith in me has been a driving force behind my perseverance and success.

DEDICATION

To my Mother, for always believing in me.

Chapter 1

INTRODUCTION

1.1 Motivation

The intent of this work is to improve robotic manufacturing processes where the elasticity of both the workpiece and the robot must be taken into account. Efficient and accurate robotic interactions with elastic structures are critical for modern manufacturing processes. For many types of robot-workpiece elastic interactions such as clamping and drilling aircraft structures, maintaining normality and limiting shear forces are essential to perform the process within acceptable tolerances [4, 5]. An example of such a structure is shown in Fig. 1.1. Out of tolerance conditions can arise as stiffness varies with location on the workpiece or by altering process parameters such as interaction speeds or applied forces. In many manufacturing processes, robots are typically limited to preprogrammed actions. In cases where the robot must interact with a structure of unknown elasticity, fixed programming limits accuracy and repeatability. These preprogrammed interactions lack the ability to accommodate variation in structural stiffness resulting in errors and inefficiency. Characterizing robotic interactions with flexible structures can allow for increased interaction speeds and accommodate process changes. The ability to perform these interactions more effectively could potentially save time and increase quality for processes where a large number of similar interactions must take place.

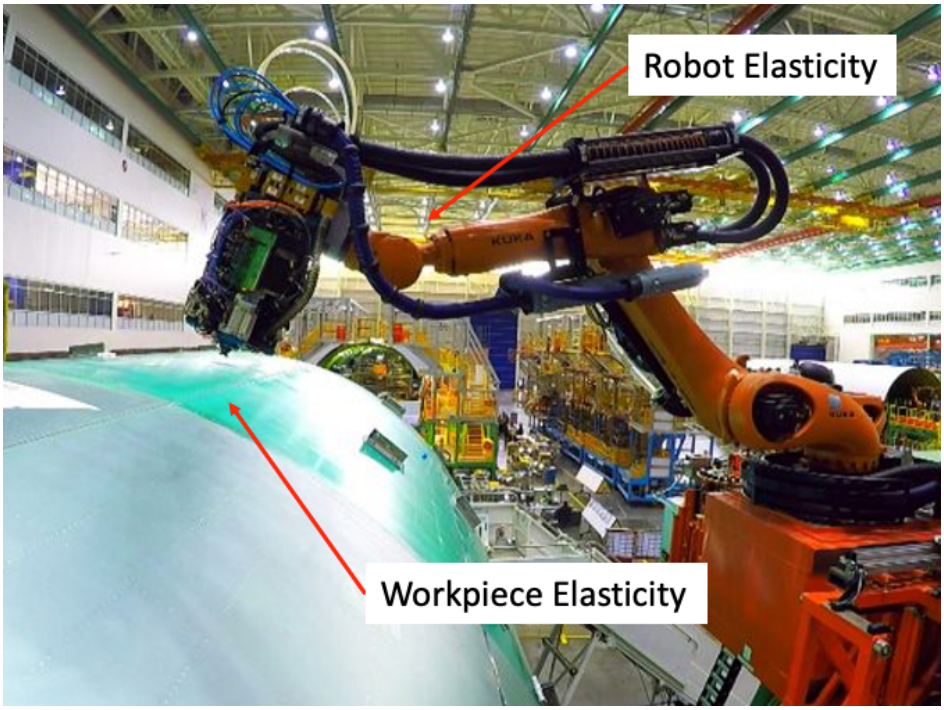

Figure 1.1: An aircraft drilling operation where the elasticity of both the robot and workpiece must be taken into account. Photo: WIRED [6]

Current methods applied to industrial robots consider elastic interactions under the assumption that the workpiece is stiff in comparison to the robot and its mounting structure, as shown in Fig. 1.2. Other works make the opposite assumption, that robot is substantially stiff in comparison to the flexible workpiece as shown in Fig. 1.3. Under this assumption, current research focuses on tasks such as grasping, folding and knot tying [7, 8]. Precision is important but not critical in such non-industrial settings. However, neither of these approaches address the needs of industrial operations such as robotic clamping and drilling on large flexible structures, where the elasticity of neither the robot nor the workpiece can be ignored.

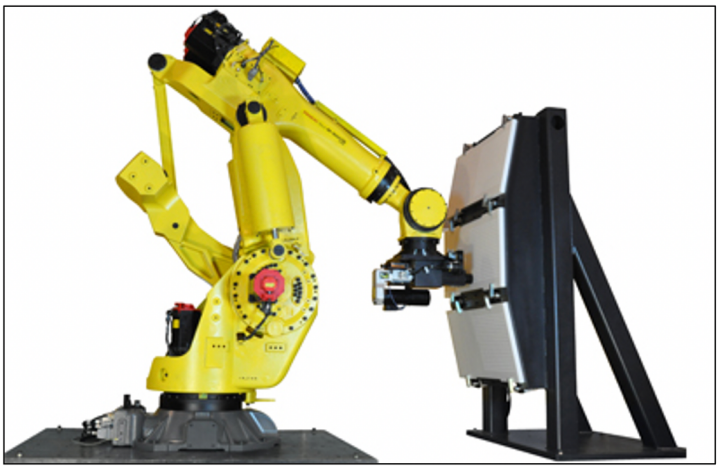

Figure 1.2: Common assumptions made about robot and workpiece relative stiffness. In this case the workpiece is considered stiff in comparison to the robot. Photo: FANUC [9]

Figure 1.3: Common assumptions made about robot and workpiece relative stiffness. In this case the robot is considered stiff in comparison to the workpiece. Photo: CORO LAB [10]

This work proposes a data-based approach that can take into account the elasticity of both the workpiece and the robot, without relying on the assumption that the workpiece is stiff in comparison to the robot or vice versa. Data-based models [11, 12], that learn the elastic interactions at relatively slow speeds, are then used to speed up similar operations. Similar approaches to collect data and use it for improved control has been developed in other machine learning applications, e.g., [13, 14, 15]. In the current application, the original interaction model obtained using slow interactions can be used to speed up the operation at the same location on the next workpiece. Moreover, data acquired using slow interactions at a few points on the workpiece can be used to speed up the operations at intermediate points.

In this work, the proposed data-based approach is applied to a robotic clamping operation as seen in Fig. 1.4, where both the elasticity of the workpiece (aluminium beam) and robot (Kinova MICO) must be taken into account. The clamping operation requires that the robot gradually apply a force normal to the workpiece until a target force is reached. The goal is to maintain normality with the workpiece and to keep the shear force within prescribed levels throughout the interaction as the robot and workpiece experience deflections.

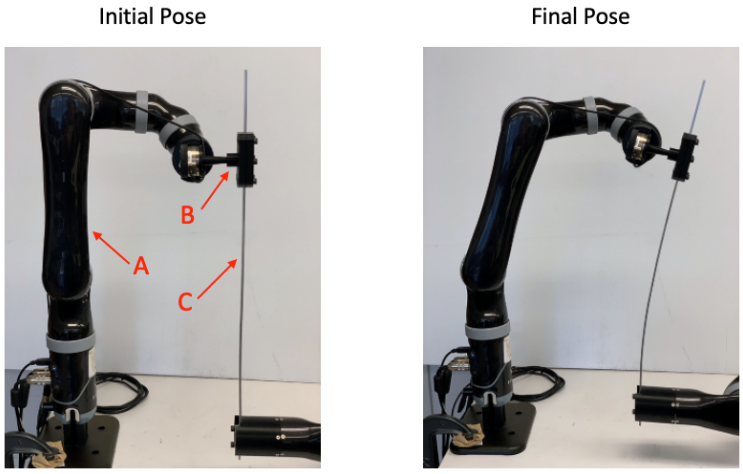

Figure 1.4: Experimental setup with elastic robot and elastic beam in contact: (A) Kinova MICO robotic arm, (B) tool contact point and (C) flexible aluminum beam. The robot is shown in the image on the left prior to performing a controlled interaction on the beam and on the right after the controlled interaction.

1.2 Problem Statement and Research Questions

Problem statement: As stated in Section 1.1, previous works on robot-workpiece interaction often rely on one of two assumptions that depend on the type and use of the robot. In the case of an industrial robot performing a manufacturing process, an assumption is made where the workpiece is modeled as having a stiffness much grater than that of the robot.

$$K_{wp} \gg K_r \tag{1.1}$$

Where K_{wp} and K_r are the relative stiffness of the workpiece and robot respectively. However if the assumption made in Eq. 1.1 is not correct and the workpiece flexes under load, accuracy cannot be maintained. Or, in the case of a robot preforming a task in a non-industrial setting, the robot is modeled as substantially stiff relative to the workpiece.

$$K_r \gg K_{wp} \tag{1.2}$$

However if the assumption made in Eq. 1.2 is not correct and the robot flexes under load, accuracy cannot be maintained. These assumptions can work well, although the challenge is that in some circumstances neither are appropriate. Such circumstances can be seen in Fig. 1.1 where the stiffness of the robot dominates the robot-workpiece interaction when force is applied in the direction normal to surface of the aircraft fuselage where the robot can easily deform the thin sheet metal skin, while at the same time the stiffness of the workpiece dominates perpendicular to that direction. Considering these circumstances, how can efficient and accurate interactions of flexible robots and flexible structures be achieved where the elasticity of the workpiece and the robot must be accounted for?

Research Questions: The subsequent research questions stem directly from the problem settlement.

RQ1 At a single location on a workpiece how can an elastic interaction between the robot and workpiece be learned and reproduced efficiently, when neither the stiffness of the robot or workpiece are known a priori?

Conventionally the elastic deformations that take place during a robot-workpiece interaction are often compensated through two main approaches used to account for interaction errors. The first is a model-based approach that takes into account the known stiffness properties of the robot and then corrects the related error in some manner [16, 17, 18]. The second is a sensor-based approach that measures the interaction with the workpiece and corrects the error by use of an algorithm or control law [19, 20, 21]. Model-based methods may not adequately capture the combined elasticity for precision operations [22], and sensor-based correction can yield precision, but could lead to slow operation speeds [23].

RQ2 How can robot-workpiece interactions at locations where interactions have not directly been learned, be efficiently predicted from a minimum number of known measurements?

Even with efficient data-based methods as discussed in **RQ1** these methods alone do not completely address all of the challenges associated with large structures where many discrete interactions must take place. Learning all of the interaction locations on a large workpiece such as an aircraft fuselage, where thousands of interactions take place would be prohibitively slow. However, it would be desirable to apply such data-based procedures to optimally learn a minimum number of interactions and then use this information to accurately predict interactions at unmeasured locations where geometric and mechanical changes may cause additional errors.

1.3 Main Contributions

The subsequent main contributions stem from and directly address the research questions in 1.2.

MC1.1 Learn and reproduce controlled interactions at measured locations even though the stiffness of the workpiece is unknown or hard to model.

This contribution addresses the research question **RQ1** and has been published in [1].

This work explores the use of a Controlled-Interaction Algorithm to learn robot-workpiece elastic interactions. Initially a heuristic based Controlled-Interaction Algorithm is employed and proven to be effective yet not very efficient. In order to reproduce controlled interactions at increased speeds, a relationship between the robot joint angles and applied normal force is found from the learned data using a nonparametric locally-weighted regression. Given a desired normal force profile in time, the data-based approach is used to generate time-based robot-joint (velocity) trajectories. From the experimental results it can be seen that such data-based approaches work well for increasing interaction speeds at learned locations on the structure.

MC1.2 Stiffness estimation based Controlled-Interaction Algorithm for control of robot-workpiece elastic interactions

This contribution addresses the research question **RQ1** and has been published in [2].

This work explores the use of a stiffness estimation based Controlled-Interaction Algorithm to learn robot-workpiece elastic interactions that improves upon the methods used in **MC1.1**. In manufacturing operations such as clamping and drilling of elastic structures, tool-workpiece normality must be maintained, and shear forces minimized to avoid tool or workpiece damage. The challenge is that the combined stiffness of a robot and workpiece, needed to control the robot-workpiece elastic interactions are often difficult to model and can vary due to geometry changes of the workpiece caused by large deformations and associated pose variations of the robot. The main contribution of this work is an algorithm, (i) to learn the robot-workpiece stiffness relationship using a model-free data-based approach and (ii) to use it for applying desired forces and torques on the elastic structure. Moreover, comparative experiments with and without

the data-based stiffness estimation show that clamping operating speed is increased by four times when using the stiffness estimation method while interaction forces and torques are kept within acceptable bounds.

MC2 With a minimum number of known measurement locations efficiently predict controlled interactions at unmeasured locations.

This contribution addresses the research question **RQ2** and has been submitted for publication as a journal article [3].

During manufacturing processes, for instance clamping and drilling elastic structures, it's crucial to maintain normality of the tool-workpiece forces for minimizing shear forces and torques to avoid tool or workpiece damage. The difficulty lies in precision model-based predictions of the relatively-large deformations as the applied force is increased, due to the robot-workpiece elastic interactions, which are needed for selecting the appropriate robot pose that ensures force normality. Therefore, recent works have used force-displacement measurements at each work location to select the robot pose for ensuring tool normality — however, such local-estimation-based approach at each work location can be slow and therefore, time prohibitive. The main contributions of this work are: (i) to use Gaussian Process Regression (GPR) methods [24] to learn the robot pose for force normality at unmeasured workpiece locations; and (ii) to use active learning for optimally selecting and minimizing the number of measurement locations needed for accurate learning of the robot-pose map with the data enabled approach. Experimental results show that the number of data points needed with active learning is 77.8% less than the case with a benchmark Linear Positioning learning for the same level of model precision. Moreover, the learned robot-pose map enables rapid increase of the normal force in the presence of elastic interactions at unmeasured locations on the workpiece, reaching speeds up to eight times faster than the original interaction speed when the robot is learning the correct pose.

1.4 Research Timeline

A summary of the research timeline is shown in Fig. 1.5

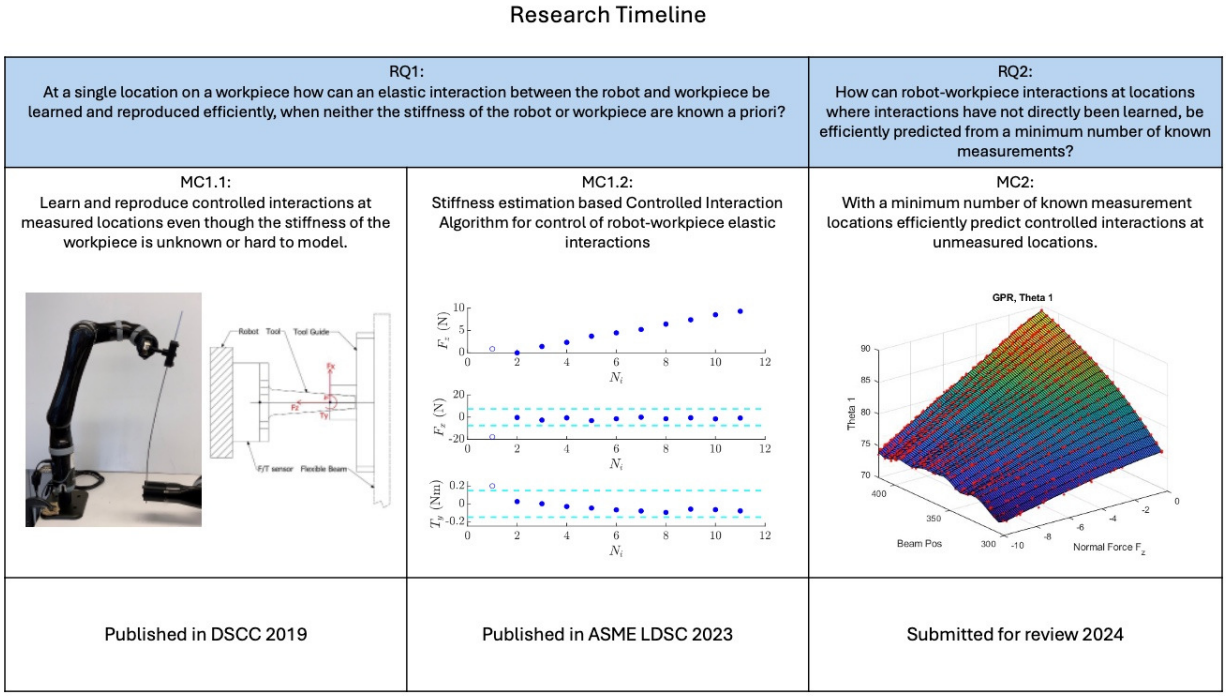

Figure 1.5: Timeline of research with research questions, main contributions and related publications [1, 2, 3].

1.5 Outline

The remainder of this dissertation is organized with the following structure. Related work and relevant literature is presented in Chapter 2. Work relating to the first part of main contribution 1 (**MC1.1**) is presented in Chapter 3, the development of Data-based learning for control of elastic interactions between a robot and workpiece. Work relating to the second part of main contribution 1 (**MC1.2**) is discussed in Chapter 4, the development of data-based stiffness estimation for control of robot-workpiece elastic interactions. Next, work relating to main contribution 2 (**MC2**) is discussed in Chapter 5, the development

of active data-enabled robot learning of elastic workpiece Interactions. Lastly, Chapter 6 presents summary of the main contributions and potential future work relating to data-based learning for control and prediction of robot-structure interactions with comparable robot and structure stiffnesses.

Chapter 2
LITERATURE REVIEW AND BACKGROUND

This chapter is comprised of a short review of available literature, and background information relevant to each of the main contributions: **MC1.1**, **MC1.2** and **MC2** presented in this dissertation. The background for each contribution is drawn from published articles [1, 2] and a submitted article [3].

2.1 Literature Review of Robot and Workpiece Stiffness Models

Elastic interactions between an industrial robot and workpiece where the stiffness of the robot and workpiece are not known however must be accounted for, is not directly addressed by present literature. As discussed in Chapter 1, current methods applied to industrial robots consider elastic interactions under one of two assumption, that the workpiece is stiff in comparison to the robot and its mounting structure or that robot is substantially stiff in comparison to the flexible workpiece.

2.1.1 Robot Stiffens Models

In 1980 J. Kenneth Salisbury developed a method for actively controlling the Cartesian stiffness of a robotic manipulator and in doing so created a rudimentary robot stiffness model [25]. This rudimentary model provides a basis for many works that follow. Zefran et al. [26] expand upon Salisbury's work by deriving a coordinate-free representation of the Cartesian stiffness matrix and Pashkevich et al. [27] provide a summary of the related works and expressions for the Cartesian stiffness matrix. Chen and Kao [28, 29] expand on the Salisbury's model by deriving the Conservative Congruence Transformation (CCT) that allows for external forces to be incorporated in to the model. Detailed examples and

application of the CCT for the stiffness control of robotic systems is provided by Li et al. [30] and Chen [31]. Methods for robot joint stiffness identification and characterization are presented by Alici and Shirinzadeh [32] as well as Dumas et al. [33]. Examples of robotic stiffness optimization in practical applications are detailed for robotic machining applications by Guo et al. [18] and for robotic drilling applications by Bu et al. [34]. Finally, an approximation method for stiffness calculation of robotic arms is provided by Sun and Fang [35].

2.1.2 Deformable Workpiece Models

With regard to the latter assumption, that robot is substantially stiff in comparison to the flexible workpiece, there is a large amount of current work relating to sensing, modeling and manipulation of deformable objects. Nadon et al. [7] present a comprehensive survey of the works relating to sensing and robotic manipulation of non-rigid objects. Additionally, Sanchez et al. [8] present as similar survey of recent works relating to manipulation and sensing of deformable objects in domestic and industrial applications. Many of these works employ similar methods to the research presented in this document. Fore example Cirillo et al. [36] use a six-axis tactile sensor for the control of linear and rotational slippage during graping tasks. Fazeli et al. [37] employ learning techniques that allow a robot to preform the complicated task of playing the game Jenga. And Caccamo et al. [38] utilize a GPR to map local deformability on a workpiece to the larger robot working environment. In addition to the above examples, the stiff robot models may provide valuable insight into optimization methods that allow for increased interaction efficiency.

2.2 MC1.1: Learn and reproduce controlled interactions at measured locations even though the stiffness of the workpiece is unknown or hard to model

In manufacturing processes, robots are typically limited to preprogrammed actions. In cases where the robot must interact with a structure of unknown elasticity, fixed programming

limits accuracy and repeatability. For many types of interactions such as clamping and drilling flexible structures, maintaining normality and limiting shear forces are essential to perform the process within acceptable tolerances [4, 5]. Out of tolerance conditions can arise as stiffness varies with location on the workpiece or by altering process parameters such as interaction speed. Preprogrammed interactions often limit the ability to accommodate variation in structural stiffness resulting in errors and inefficiency. Characterizing robotic interactions with flexible structures can allow for increased interaction speeds and accommodate process changes. The ability to perform these interactions more effectively could potentially save time and increase quality for processes where a large number of similar interactions must take place.

Current methods in industrial robotics consider elastic interactions under the assumption that the workpiece is stiff in comparison to the robot. The elastic deformations in the robot are then compensated through two main approaches used to account for interaction errors. The first is a model-based approach that takes into account the known stiffness properties of the robot and then corrects the related error in some manner [16, 17, 18]. The second is a sensor-based approach that measures the interaction with the workpiece and corrects the error by use of an algorithm or control law [19, 20, 21]. Other recent works make the opposite assumption that robot is substantially stiff in comparison to the flexible workpiece. Under this assumption, current research focuses on tasks such as grasping, folding and knot tying [7, 8]. Precision is important but not critical in such non-industrial settings. However, neither of these approaches address the needs of industrial operations such as robotic clamping and drilling on large flexible structures, where the elasticity of neither the robot nor the workpiece can be ignored. Model-based methods may not adequately capture the combined elasticity for precision operations [22], and sensor-based correction can yield precision, but could lead to slow operation speeds [23].

We propose a data-based approach that can take into account the elasticity of both the workpiece and the robot, without relying on the assumption that the workpiece is stiff in comparison to the robot or vice versa. Data-based models[11, 12], that learn the elastic

interactions at relatively slow speeds, are then used to speed up similar operations. Similar approaches to collect data and use it for improved control has been developed in other machine learning applications, e.g., [13, 14, 15]. In the current application, the original interaction model obtained using slow interactions can be used to speed up the operation at the same location on the next workpiece. Moreover, data acquired using slow interactions at a few points on the workpiece has the potential to be used to speed up the operations at intermediate points.

In this initial work, the proposed data-based approach is applied to a robotic clamping operation, where both the elasticity of workpiece and robot must be taken into account. The clamping operation requires that the robot gradually apply a force normal to the workpiece until a target force is reached. The goal is to maintain normality with the workpiece and to keep the shear force within prescribed levels throughout the interaction as the robot and workpiece experience deflections.

2.3 MC1.2: Stiffness estimation based Controlled-Interaction Algorithm for control of robot-workpiece elastic interactions

In manufacturing processes such as clamping and drilling of elastic structures, maintaining normality and bounding the shear forces between the robot and the workpiece are essential to avoid damage of the tool or workpiece, [4, 5, 39]. However, maintaining normality and shear forces within required process tolerances can be challenging when the stiffness of the robot-workpiece interaction is variable, which can arise due to nonlinear elastic characteristics of the robot and workpiece, large deformation of the workpiece, and location-dependent interactions with the workpiece. The current use of robots in industrial manufacturing processes often use preprogrammed actions [40, 41], which limits the accuracy of such robots when interacting with structures of unknown or varying stiffness. Therefore, the characterization of robot-workpiece interactions is necessary to accommodate stiffness variations for maintaining normality and small shear forces within process tolerances.

Existing methods for robot-workpiece interactions in industrial robotics conventionally

assume that the stiffness of the workpiece K_{wp} is much greater than the stiffness of the robot K_r, i.e., $K_{wp} \gg K_r$. Therefore, the elastic deformation only in the robot is compensated during interaction, which is achieved using two main approaches. First is a model-based approach, where a stiffness model of the robot is used to compensate robot motion error during interactions, as in [17, 18, 34, 42]. Second is a sensor-based approach, where the interaction error between robot and workpiece is monitored in real time and used as feedback to correct the robot motion using a control policy or algorithm [20, 43, 44]. Typical model-based approaches require accurate robot stiffness models, which might be difficult to obtain and furthermore, these approaches are not applicable for precision operations when both the robot and the workpiece are flexible, [45]. The sensor-based approaches can be applied to specific robot-workpiece interactions for improving precision. Sensor-based approaches are often employed with industrial robots, for example ABB and Kuka use force measurements to improve robot-workpiece interactions in low material-removal-rate processes like grinding and polishing [46], and ongoing research also seeks to increase the accuracy of robot-workpiece interactions through sensor-based feedback and control [39, 47]. Nevertheless, the range of industrial applications is still limited by the achievable accuracy, e.g., [48]. Additionally, some of the positioning errors can be corrected using onsite calibration, e.g., [49]. However, environmental variations such as part stiffness can influence the calibration of the robot [50, 51], and multiple recalibration of the robot can be cost and time prohibitive.

Previous work has considered the case where both the robot and workpiece are elastic, for a robotic clamping operation [1]. The clamping operation requires a gradual increase in the normal force until a target force is achieved, while keeping the shear force within a tolerance level. The heuristic iterative-correction algorithm in [1] uses an inverse kinematics model of the robot to make iterative corrections of the end-effector position to reduce shear forces and achieve normality. A limitation of the heuristic algorithm is that a large number of iterations might be needed since the iterative corrections do not estimate nor account for the stiffness of the robot and the workpiece. The current work proposes a model-free approach that uses an online estimation of the combined stiffness between the robot (Kinova

MICO) and workpiece (aluminium beam) for corrective motion of the robot. Experimental results show that the stiffness-estimation-based approach achieves a target normal force in four times fewer iterations, compared to the heuristic approach without using the stiffness estimation.

2.4 MC2: With a minimum number of known measurement locations efficiently predict controlled interactions at unmeasured locations

In manufacturing operations utilizing industrial robots for clamping and drilling flexible structures, it is vital to maintain normality and avoid large shear forces and torques between the robot and the workpiece in order to prevent damage to the tool or workpiece [4, 5, 39]. However, maintaining normality and controlling shear forces within required tolerances becomes challenging when the stiffness of the robot-workpiece interaction varies. This variation can be attributed to the nonlinear elastic characteristics of both the robot and workpiece, substantial deformation of the workpiece, and location-dependent interactions (such as those outlined in Appendix A). The prevalent use of preprogrammed interactions in current industrial manufacturing processes [40, 41] limits precision when dealing with structures of unknown or varying stiffness. Therefore, learning the robot pose corrections during robot-workpiece interactions is imperative to accommodate stiffness variations, ensure normality of the applied forces and maintain shear forces and torques within specified process tolerances.

Traditional approaches to robot-workpiece interactions with industrial robotics typically assume that the workpiece's stiffness is significantly higher than that of the robot. Hence, compensation of elastic deformation in the robot during the interaction is accomplished through the implementation of two primary approaches. The first approach involves using a model-based method, wherein a stiffness model of the robot is employed to correct errors in robot motion during interactions, [17, 18, 34, 42]. The second approach involves sensors, wherein real-time monitoring of the interaction error between the robot and workpiece is conducted. This information serves as feedback to adjust the robot's motion through the application of a control strategy or algorithm, [20, 43, 44]. Conventional model-based

methods necessitate precise robot stiffness models, which can be challenging to acquire. Additionally, these approaches prove impractical for precision tasks involving both flexible robot structures and flexible workpieces, [45]. Sensor-based methods are commonly utilized in conjunction with industrial robots. For example, force measurements are employed to manage interactions between robots and workpieces in processes with low material removal rates, [46]. Recent research also aims to improve the accuracy of robot-workpiece interactions through sensor-based methods in more general applications, [39, 47, 48]. Moreover, on-site calibration, as suggested in [49], can address certain positioning errors although variation of the workpiece stiffness may impact the robot's calibration [50, 51] and conducting multiple recalibrations could be both cost and time prohibitive.

Prior research has explored scenarios involving both the robot and workpiece exhibiting elasticity in the context of a robotic clamping operation [1], where iterative corrections of the robot pose is used to gradually increase the normal force until a specified target force is attained, while ensuring that the shear force remains within an acceptable tolerance range. Moreover, the convergence of the iterative procedure can be sped up (about about 4 times) if local stiffness is estimated from the measurements, [2]. However, such local iterative methods are still slow if the correct robot pose needs to be relearned at each location where work needs to be done. This motivates the proposed learning of the robot pose (joint angles) for the unmeasured workpiece locations by utilizing data from previous work locations using the Gaussian Process Regression (GPR) approach, [52]. Additionally, active learning is used to minimize the number of measured workpiece locations where such data needs to be collected for sufficient precision in the robot-pose map for operations at other locations. Experimental results show that the active data-based modeling method requires 77.8% fewer measurement locations when compared to a linear-positioning-based approach that does not use active data-based modeling. Additionally, the learned robot-pose map allows for rapid increase of the normal forces at unmeasured workpiece locations, up to eight times the iterative method speed.

Chapter 3

DATA-BASED LEARNING FOR CONTROL OF ELASTIC INTERACTIONS BETWEEN ROBOT AND WORKPIECE

This chapter addresses the main contribution **MC1.1**; *Learn and reproduce controlled interactions at measured locations even though the stiffness of the workpiece is unknown or hard to model*, and has been published in [1]. The main contribution of this chapter is to show experimentally, that data acquired during a robotic clamping operation can be used to speed up the process for similar operations. Utilizing the learned parameters, a map between the measured forces and robot joint positions is used to develop time-based robot-joint (velocity) trajectories to achieve a specified robot-workpiece interaction.

The contents of this chapter are organized as follows. A description of the experiment, initial heuristics-based controlled-interaction algorithm, time to joint velocity mapping as well as details of the reproduced measured interaction are presented Section 3.1. Results and discussion of the experiment are presented in Section 3.2. Lastly, conclusions are presented in Section 3.3.

3.1 Methods

This section describes the data-based robotic clamping operations as well as details of the experimental system. The methods section consists of the following four parts.

1. The experimental setup used for the clamping operations.

2. A controlled interaction with a flexible beam that allows for interaction forces and joint angles to be managed and recorded.

3. Creation of a data-based map (a model) that relates the measured forces and joint

angles and using it to develop time-based robot-joint (velocity) trajectories that achieve a specified robot-workpiece interaction.

4. Reproducing the measured interaction while varying interaction speed.

3.1.1 Experiment

The experimental setup is pictured in Fig. 3.1 and consists of a Kinova MICO robotic arm, ATI Mini 45 F/T (force-torque) sensor, 3D printed tool and 3D printed tool guide rigidly attached to a flexible beam made from 6061-T6 aluminum. The beam is 18.9mm wide, 3.15mm thick and the distance from the mounting point to the tool contact point can be adjusted. In the initial pose position in Fig. 3.1 the stiffness of the robot is 5.17N/mm in the horizontal direction and 6.30N/mm in the vertical direction. Additionally the stiffness of the beam (including mount) is 0.18N/mm in the horizontal direction and 10.12N/mm in the vertical direction. In order to measure the interaction forces and torque, the F/T sensor is attached between the end of the robotic arm and the 3D printed tool as shown in Fig. 3.2. When the tool is in contact with the tool guide, a firm connection is made between the robot and the flexible beam. The robotic arm is posed allowing for the tool to be positioned in the same plane as the beam deflection with sufficient degrees of freedom to perform the interaction, as illustrated in Fig. 3.1. Additionally it is assumed that as the beam deflection increases through the clamping operation, the corresponding normal force F_z in Fig. 3.2 will also increase.

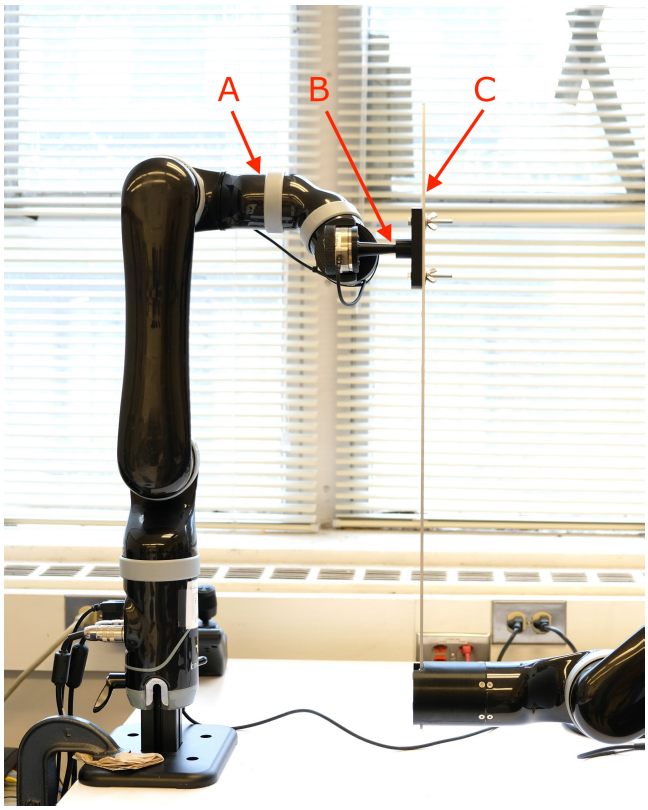

Figure 3.1: Experimental setup with the robot and flexible beam in contact: (A) Kinova MICO robotic arm, (B) tool contact point and (C) flexible aluminum beam. A detailed schematic of the contact point is provided in Fig. 3.2.

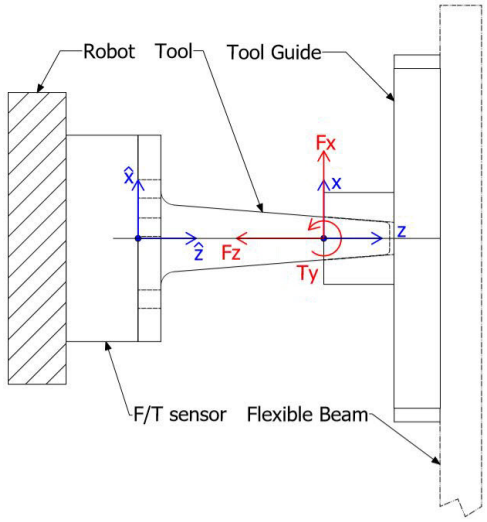

Figure 3.2: Schematic of tool contact point with the flexible beam from Fig. 1.4, and the F/T (force/torque) sensor with original coordinate frame $(\hat{z}, \hat{x})$ and shifted coordinate frame (z, x). The normal force F_z, shear force F_x and torque T_y are shown at the contact point.

3.1.2 Heuristics-Based Controlled-Interaction Algorithm

The first stage of the experiment is designed to be a controlled-interaction that is representative of a robotic clamping operation with a flexible structure. We define successful clamping to be the application of a prescribed normal contact force, while simultaneously maintaining only small shear force and torque. The goal of this first step is to discover the static relationship between the motion of the robot while in contact with the flexible structure, and the corresponding forces and torque at the point of contact. During this process the robot moves to increase the normal force incrementally. For each normal force increment, the shear force and torque are minimized in an iterative manner. The process continues until the measured normal force F_z exceeds the required force $\tilde{F}_z = 10N$ and the shear force F_x and the torque T_y are below the corresponding thresholds $|\tilde{F}_x| = 2N$ and $|\tilde{T}_y| = 0.05Nm$, respectively. Details of the iteration are provided in Fig. 3.3. At every step in the process the forces and torques, F_z, F_x and T_y as well as robot joint angles θ_1, θ_2 and θ_3 are measured and recorded. An outline of the iterative process is presented below and in detail in Algorithm

2.

Outline of the Heuristics-Based Controlled-Interaction Algorithm:

1. Initialize the algorithm: set the target normal force $\tilde{F}_z$, shear force threshold value $\tilde{F}_x$, torque threshold value $\tilde{T}_y$ and distance to move tool each step Δz.

2. Move tool forward a small distance Δz in the z direction.

3. Record the resultant F_z, T_y, F_x, θ_1, θ_2 and θ_3.

4. In a loop, correct the torque T_y by rotating the tool around the y axis and correct the shear force F_x by moving in the x direction. This operation is repeated until both $|T_y|$ and $|F_x|$ are below the torque threshold value $\tilde{T}_y$ and shear force threshold value $\tilde{F}_x$.

5. Record the resultant F_z, T_y, F_x, θ_1, θ_2 and θ_3.

6. Repeat steps 2-4 until F_z exceeds the target normal force $\tilde{F}_z$.

Algorithm 1 Heuristics-Based Controlled-Interaction Algorithm

Require: The tool is in contact with the tool guide as shown in Fig. 3.1 and the beam is unloaded.

Initialize:
Set target normal force: $\tilde{F}_z$
Set shear force threshold value: $\tilde{F}_x$
Set torque threshold value: $\tilde{T}_y$
Set distance to move tool: Δz
Loop:
while $F_z < \tilde{F}_z$ **do**
  Record: F_z, T_y, F_x, θ_1, θ_2 and θ_3
  Move tool forward Δz in the z direction
  Record: F_z, T_y, F_x, θ_1, θ_2 and θ_3
  Loop:
  while $(|T_y| > \tilde{T}_y)$ *or* $(|F_x| > \tilde{F}_x)$ **do**
    Loop:
    while $|T_y| > \tilde{T}_y$ **do**
      Correct torque by rotating the tool around the y axis.
      Record: F_z, T_y, F_x, θ_1, θ_2 and θ_3
    end while
    Loop:
    while $|F_x| > \tilde{F}_x$ **do**
      Correct shear by moving in the x direction.
      Record: F_z, T_y, F_x, θ_1, θ_2 and θ_3
    end while
  end while
end while

The measured F_z, F_x and T_y from the controlled-interaction can be seen in Fig. 3.3. Points in red indicate when the robot is about to be incremented forward $\Delta z = 2mm$. Between each increment (red points), the process required about six iterations (shown in blue) for the torque and shear force to become small. The iterations required between the froward increments tend to limit the process and it is desirable to perform as few iterations as possible. Overall, the process is slow, and takes about 280 seconds.

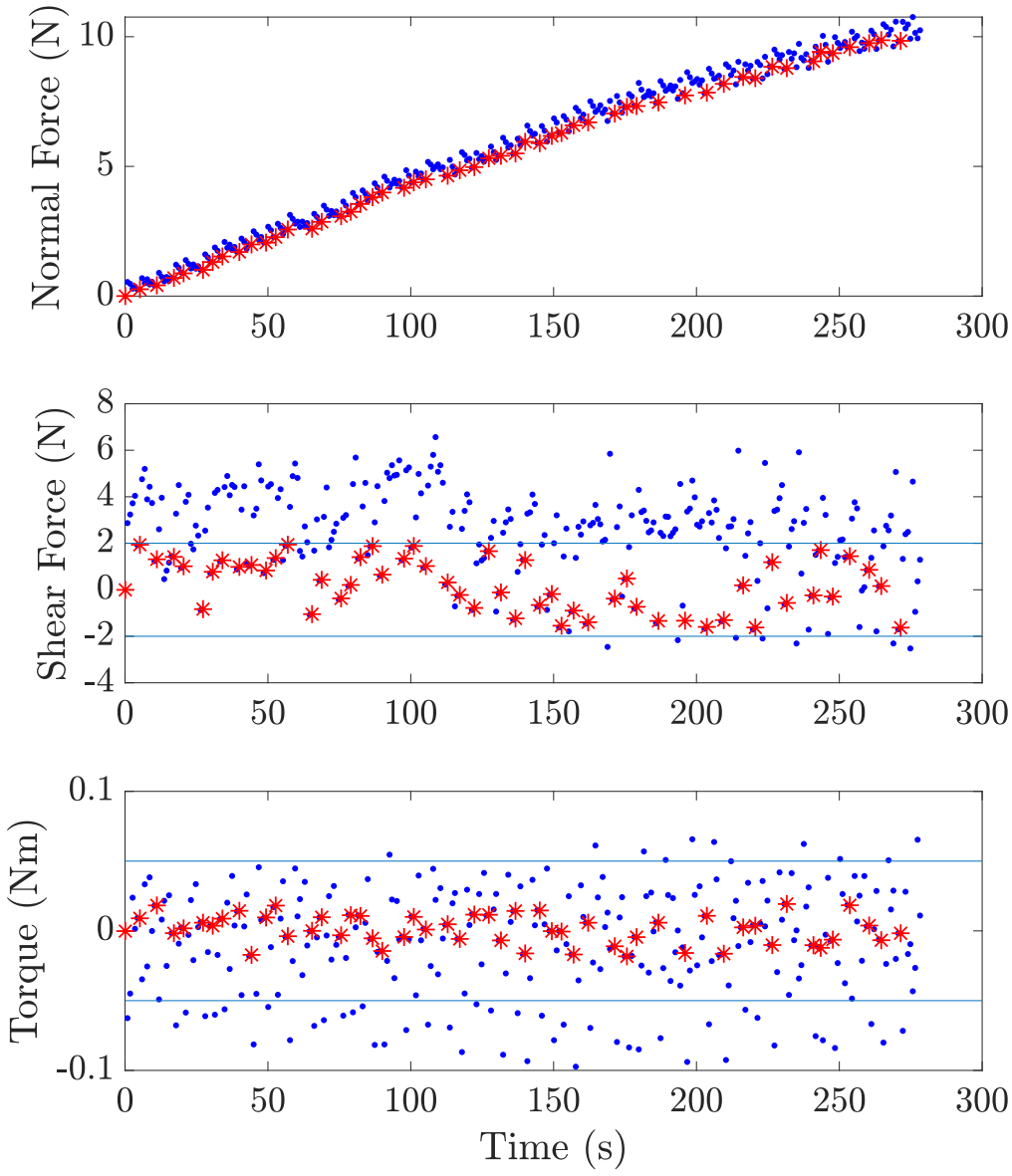

Figure 3.3: Measured forces and torque from the heuristics-base controlled-interaction with the beam. The Points in red indicate when the robot is about to be incremented forward as the torque and shear force have become small. On an average, six iterations are present in blue between the forward increments.

3.1.3 Joint Velocity-Trajectory Generation

In order to produce the desired time-based robot-joint (velocity) trajectories, a joint angle vs. normal force relationship must first be established. The relationship between the controlled-interaction joint angle and the normal force is found from the experimental data using a nonparametric locally-weighted regression. The data used in the fit are the red points in Fig. 3.3 where the tool is sufficiently normal to the flexible beam ($|T_y| > \tilde{T}_y$) and the shear force is acceptably small ($|F_x| > \tilde{F}_x$). While several regression methods could be used, the Locally Estimated Scatterplot Smoothing (LOESS) approach is used in the current work because, in general, the nature of the interaction is not known and may exhibit nonlinearities arising from changing interaction elasticity as well as nonlinear robot kinematics [53]. Figure 3.4 shows the normal forces that are used to create the joint angle trajectories and the fit obtained with the LOESS regression.

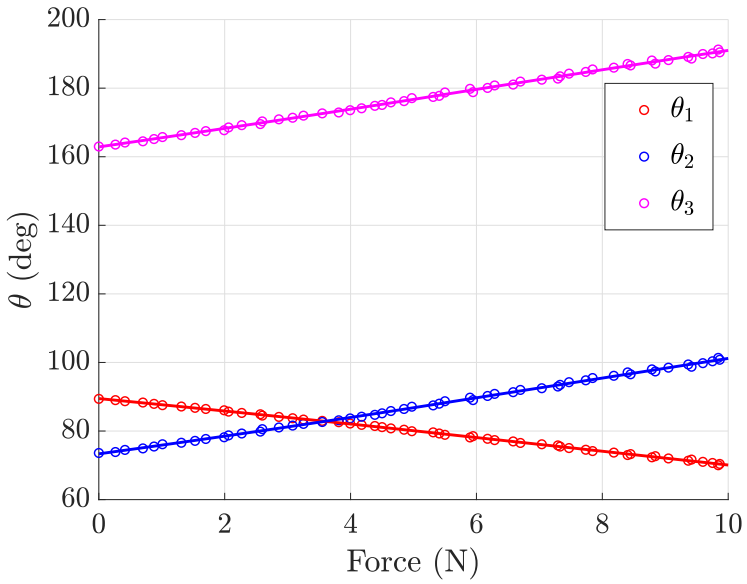

Figure 3.4: Robot joint angle, normal force mapping created by applying the LOESS regression to the red data points from Fig. 3.3 where torque and shear force are small.

Given any desired normal-force profile in time, the data-based approach can be used to generate the desired time-based robot-joint (velocity) trajectories. For this experiment, a sigmoidal relationship between normal force and time is employed as shown in Fig. 3.5. The sigmoidal relationship is used so that the applied normal force changes smoothly in time, which avoids abrupt changes in the interaction force and torque. Mapping the normal-force trajectory through the learned LOESS normal force joint angle relationship and taking the time derivative produces the desired time joint velocity relationship as can be seen in Fig. 3.6.

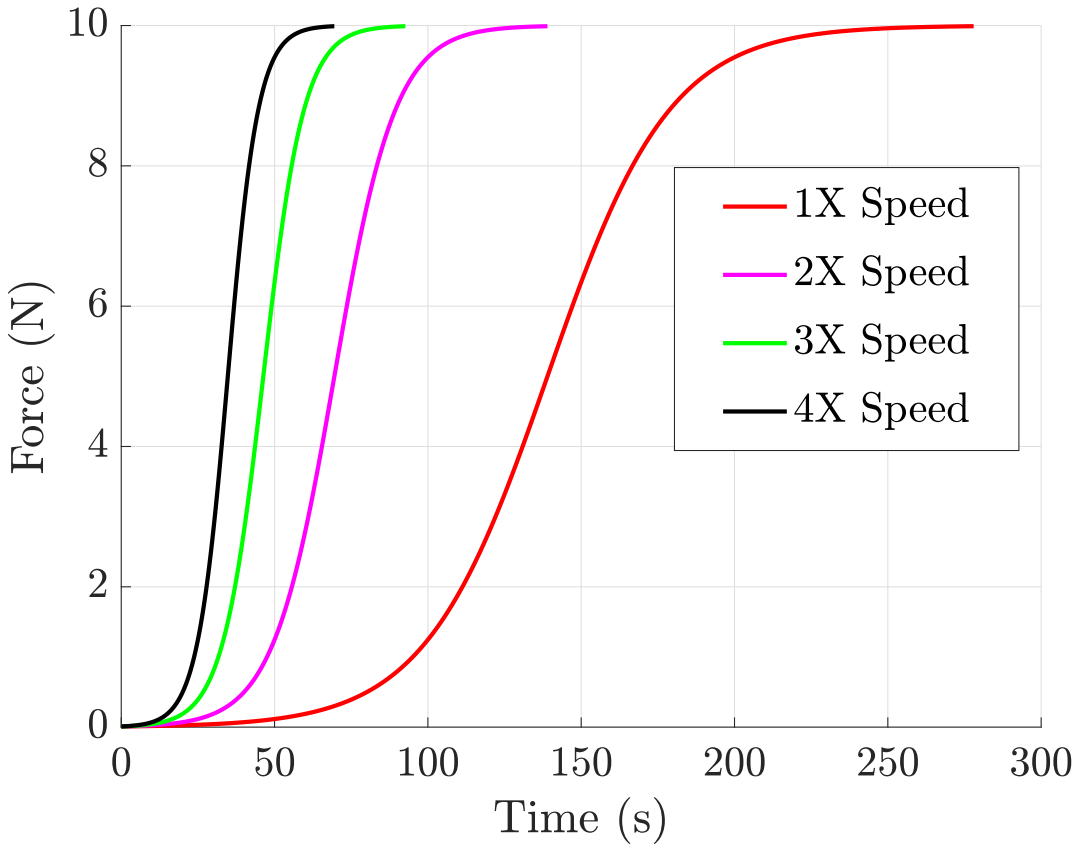

Figure 3.5: Prescribe sigmoidal normal force profiles as a functions of time. Used to reproduce the robot-beam interaction at various speeds.

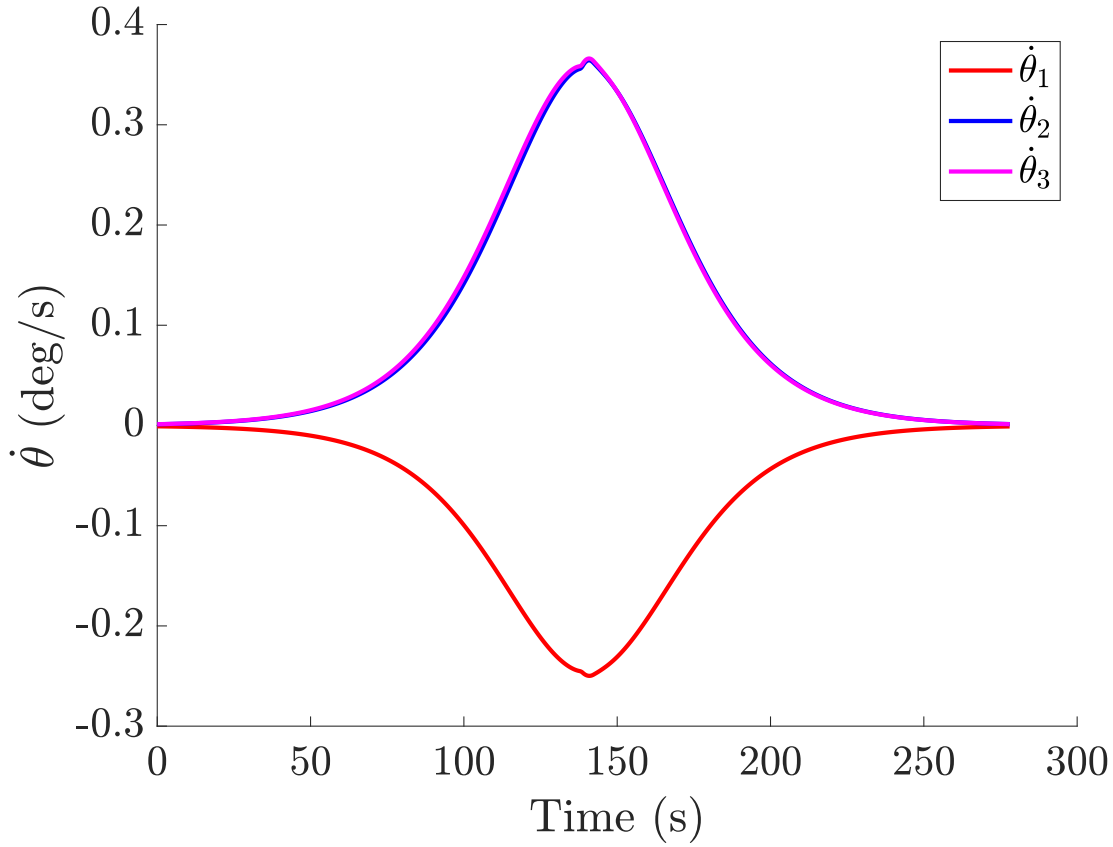

Figure 3.6: Time-based robot-joint (velocity) trajectories formed by mapping the normal force time sigmoid through the learned LOESS normal force joint angle relationship and taking the time derivative.

3.1.4 Reproducing the Measured Interaction

The robot beam interaction is reproduced by commanding the robot to move with the prescribed joint velocities. In order to determine the limits of the interaction, the speed is increased by scaling the sigmoid as seen in Fig. 3.5 and repeating the experiment. Forces and torque are measured during the interaction to determine if they stay within acceptable limits.

3.2 Results And Discussion

Results of the reproduced interactions are evaluated against the original controlled-interaction to determine the performance of the data-based prescription of the robot-joint (velocity) trajectories. A reproduced interaction is determined to be unacceptable when the measured torque or force exceeds twice the threshold of $\tilde{T}_y$ or $\tilde{F}_x$ from the learning algorithm, $|T_y| > 0.1Nm$ and $|F_x| > 4N$ respectively.

3.2.1 Reproduced Robot-Beam Interaction

The measured normal forces F_z for each reproduced robot-beam interaction are plotted in Fig. 3.7. Four increasing interaction speeds of $1X, 2X, 3X$ *and* $4X$ the original speed are shown. As expected the normal force F_z follows a sigmoidal path for each of the interaction speeds and the maximum value of the normal force F_z reaches an acceptable steady state force of $\approx 91\%$ *to* 96% the target $10N$ force.

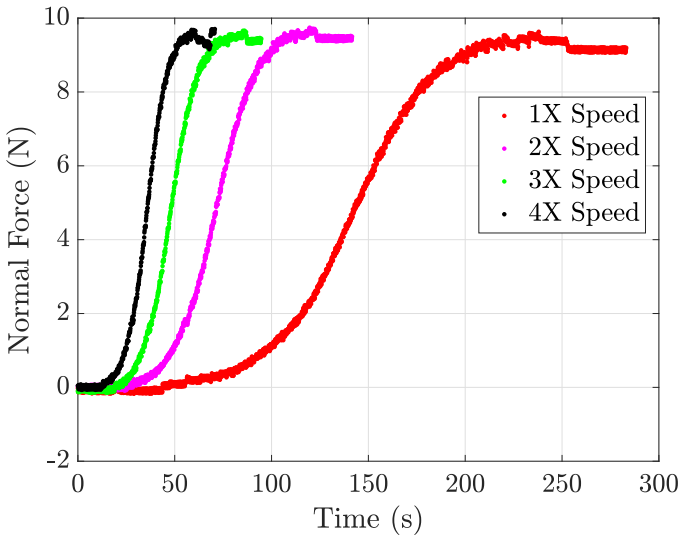

Figure 3.7: Measured normal force as speed is increased for the original robot-beam configuration.

Interaction torques T_y for each reproduced interaction are plotted in Fig. 3.8. As interaction speeds are increased the torque T_y remains well within the acceptable range of $\pm 0.1 Nm$. Consequently, tool normality with the workpiece is maintained up to $4X$ the original interaction speed.

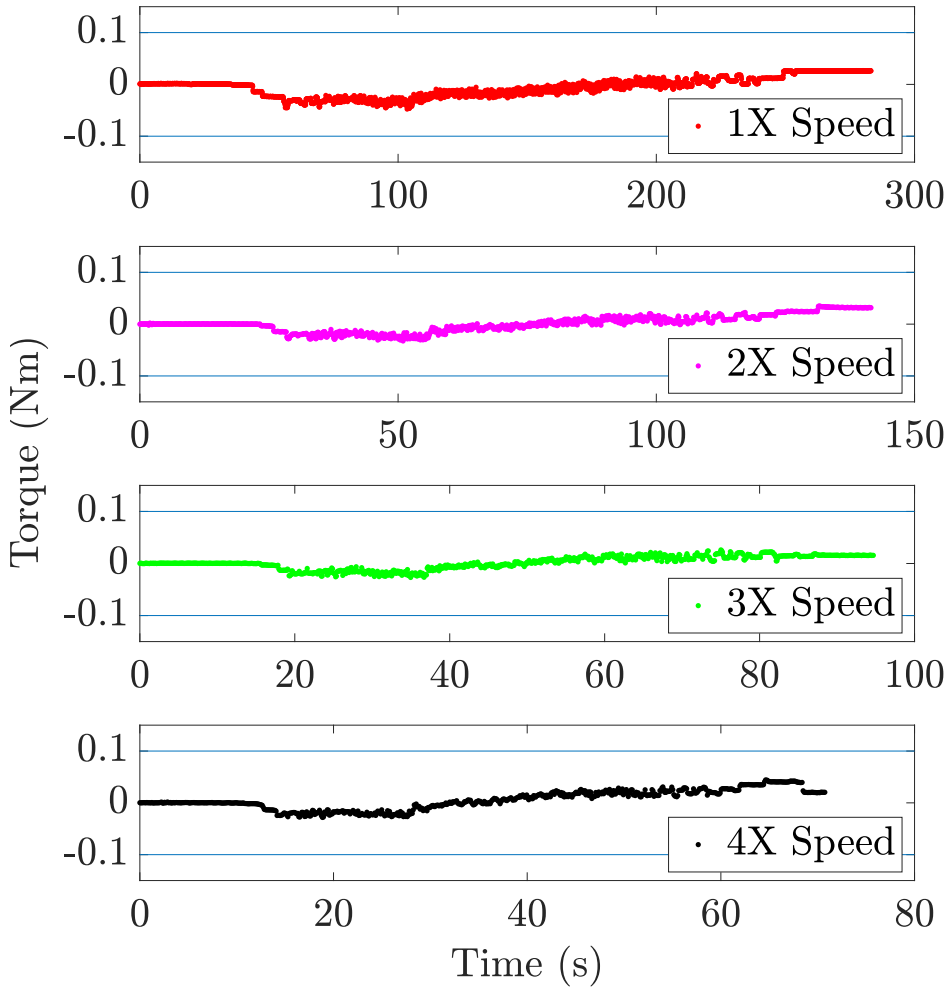

Figure 3.8: Measured interaction torque as speed is increased for the original robot-beam configuration. Acceptable interaction torque limits are indicated by the blue lines.

Shear forces F_x for each reproduced interaction are plotted in Fig. 3.9. As the interaction speeds are increased, the shear force F_x trends toward the lower limit of the acceptable range of $\pm 4N$. At $4X$ the original interaction speed F_x exceeds the acceptable range near the end of the interaction.

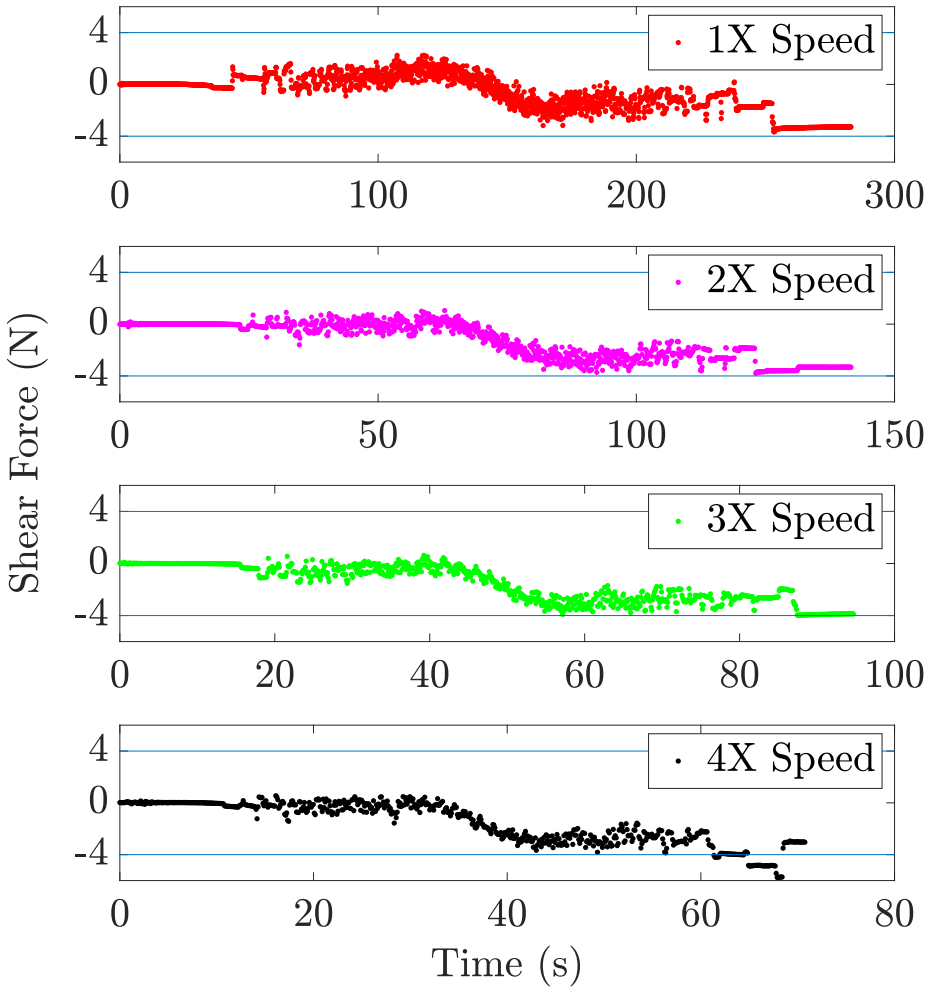

Figure 3.9: Measured shear force as speed is increased for the original robot-beam configuration. Acceptable shear force limits are indicated by the blue lines.

Based on the experimental results, the data-based approach can be used to increase the speed by 3 times that of the sensor controlled-interaction before the shear forces become unacceptable. This reproduced interaction takes about 93s and results in a significant time savings of 187s.

3.3 Chapter Conclusions

This experimental effort showed that robotic interactions with flexible structures can be learned through data-based methods. Moreover, the results show that the learned data-based model can be used to substantially increase the operating speed, while maintaining tool-workpiece interactions at acceptable levels. The increased speed represents a significant time-savings in the manufacturing process. The potential to substantially increase the operating speed in the experimental results suggest that further research should be pursued, such as attempting to estimate the data-based map at discrete locations and then infer the tool-workpiece interactions at other locations where controlled-interactions have not been previously conducted.

Chapter 4

DATA-BASED STIFFNESS ESTIMATION FOR CONTROL OF ROBOT-WORKPIECE ELASTIC INTERACTIONS

This chapter addresses the main contribution **MC1.2**; *Stiffness estimation based Controlled-Interaction Algorithm for control of robot-workpiece elastic interactions*, and has been published in [2]. The main contribution of this chapter is an algorithm, (i) to learn the robot-workpiece stiffness relationship using a model-free data-based approach and (ii) to use it for applying desired forces and torques on the elastic structure.

The rest of this chapter is organized as follows. A description of the experiment, without stiffness-estimation (initial heuristics-based controlled-interaction algorithm) and with stiffness-estimation (stiffness-based controlled-interaction algorithm) are presented in Section 4.1. Results and discussion of the experiment are presented in Section 4.2. Lastly, conclusions are presented in Section 4.3.

4.1 Methods

4.1.1 Experiment

The controlled interaction studied in this paper is representative of a robotic clamping operation with a flexible structure. A successful clamping operation is the application of a prescribed normal contact force, while maintaining small shear force and torque to avoid tool and/or structure damage. Additionally, the shear force and torque at the contact point need to remain small while the normal force is increased. This is challenging because the robot pose can change substantially during the process due to large deflection of the structure

as shown in Fig. 4.1.

The experimental setup is shown in Fig. 4.1, which consists of a Kinova MICO robotic arm with a ATI Mini 45 six degrees of freedom force-torque (F/T) sensor mounted on the end-effector. The robot's end-effector is firmly attached to the beam using a 3D-printed tool and guide, as shown in Fig. 4.2, where the the F/T sensor is placed between the robotic arm and the 3D-printed tool. The F/T sensor has a maximum measurement errors of $F_z = 1.00\%$, $F_x = 1.25\%$ and $T_y = 1.50\%$ at a 95% confidence level. The beam is made from 6061-T6 aluminium and has $18.9mm$ width, $3.15mm$ thickness and the distance from the mounting point to the tool contact point is $415mm$. The initial pose of the robot allows for sufficient degrees of freedom to perform the interaction goal of increasing the normal force to a desired set point, while maintaining low shear and torque at the tool contact point. Additionally it is assumed that as the beam deflection increases through the clamping operation, the corresponding normal force F_z in Fig. 4.2 will also increase.

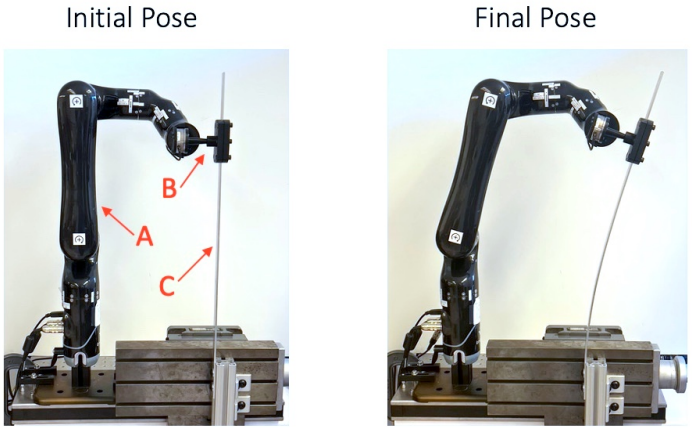

Figure 4.1: Experimental system. The robot, Kinova MICO (A), applies a load using a tool (B) on a flexible aluminum beam (C). The interaction leads to substantial deflection in the beam as seen by comparing the initial pose (left image) and the final pose (right image).

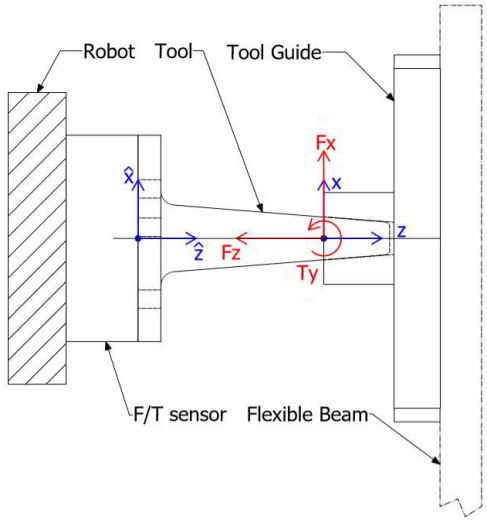

Figure 4.2: Schematic of the tool contact contact point. The normal force F_z needs to be increased to a specified value while the shear force F_x and torque T_y at the contact point need to be minimized to avoid tool or workpiece damage. The forces are measured using a force-torque (F/T) sensor where the original coordinate frame of the sensor $(\hat{z}, \hat{x})$ and shifted coordinate frame of the tool tip (z, x) are shown.

4.1.2 Interaction Algorithm Without Stiffness Estimation

The heuristic interaction algorithm from [1] is an iterative correction process using only force measurements without stiffness estimation. During this process the normal force is increased incrementally by moving the robot forward in the **z** direction along the tool axis by Δz, producing a change in normal force ΔF_z. The interaction is determined to be acceptable when the measured torque and shear force are within the threshold values. Thus for each increment, the shear force and torque are minimized to stay within the force and torque thresholds by moving the tool in the **x** direction and rotating around the **y**-axis, in an iterative manner. Once the tool tip shear force and torque are within the desired thresholds, the incremental displacement along the **z**-axis continues until the measured normal force F_z reaches the required force $\tilde{F}_z = 10N$ and the shear force F_x and the torque T_y are below the

corresponding thresholds. The iterative algorithm is outlined in Algorithm 2.

The threshold values for shear force and torque are selected based on the force and torque values measured at the smallest-size joint motion of the robot. For example, each joint of the robot $(\theta_1, \theta_2, \theta_3)$ is moved by ϵ rad, where ϵ is the smallest command for each joint angle. The resulting contact shear force and torque magnitudes (averaged over five trials) provide threshold values for shear force as $|\tilde{F}_x| = 7.5N$ and torque $|\tilde{T}_y| = 0.15Nm$, in this application.

Algorithm 2 Interaction Without Stiffness Estimation from [1]

Require: The tool is in contact with the tool guide as shown in Fig. 4.1 and the beam is unloaded.

Initialize:
Set target forces and torque: $\tilde{F}_z$, $\tilde{F}_x$ and $\tilde{T}_y$
Set distance to move tool: Δz
Set minimum correction distance: μ
Set minimum correction angle: ϵ
Loop:
while $F_z < \tilde{F}_z$ **do**
  Record: F_z, T_y, F_x, θ_1, θ_2 and θ_3
  Move tool forward Δz in the z direction using inverse kinematics in Eq. (4.3)
  Record: F_z, T_y, F_x, θ_1, θ_2 and θ_3
  Loop:
  while $(|T_y| > \tilde{T}_y)$ *or* $(|F_x| > \tilde{F}_x)$ **do**
    Loop:
    while $|T_y| > \tilde{T}_y$ **do**
      Correct torque by rotating the tool around the y axis as in Eq. (4.1)
      Record: F_z, T_y, F_x, θ_1, θ_2 and θ_3
    end while
    Loop:
    while $|F_x| > \tilde{F}_x$ **do**
      Correct shear force by moving in the x direction as in Eq. (4.2)
      Record: F_z, T_y, F_x, θ_1, θ_2 and θ_3
    end while
  end while
end while

Iterative correction: As the robot moves forward in the z direction at each increment, the shear force and torque at the contact point between the tool and the beam can change since the tool does not necessarily remain normal to the surface of the beam due to the additional deflection of the robot and workpiece. The robot corrects for the change in shear force and torque by moving the tool tip.

Step 1. Torque correction: The robot minimizes torque T_y at the tool tip by rotating the tool tip around the **y**-axis in the opposite direction by the smallest command angle $\epsilon = 0.005$rad (established using the date presented in Appendix B), until the measurement is below the threshold $|\tilde{T}_y| = 0.15Nm$, i.e.,

$$\Delta\theta_y = -\text{sign}(T_y)\epsilon \text{ rad.} \tag{4.1}$$

Step 2. Shear force correction: Similarly, after correcting for torque, the robot minimizes shear force F_x by moving the tool in Cartesian space in the opposite direction of the shear force by $\mu = 1mm$ (which the smallest distance command to the robot corresponding to the smallest joint angle move ϵ) until the measurement is below the threshold $|\tilde{F}_x| = 7.5N$, i.e.,

$$\Delta x = -\text{sign}(F_x)\mu \text{ mm.} \tag{4.2}$$

Inverse kinematics: Desired movement in the tool's coordinate frame is achieved using inverse kinematics of the planar 3-link robot as,

$$\Delta\boldsymbol{\Theta} = \boldsymbol{J}(\boldsymbol{\theta})^{-1}\Delta\mathbf{P}, \tag{4.3}$$

where $\Delta\boldsymbol{\Theta} = \begin{bmatrix}\Delta\theta_1 & \Delta\theta_2 & \Delta\theta_3\end{bmatrix}^T$, $\Delta\mathbf{P} = \begin{bmatrix}\Delta z & \Delta x & \Delta\theta_y\end{bmatrix}^T$ are change in joint angles and change in end-effector (tool) position respectively, and $\boldsymbol{J}(\boldsymbol{\theta}) \in \mathbb{R}^{3\times3}$ is the robot's Jacobian

matrix.

4.1.3 Interaction Algorithm With Stiffness Estimation

The interaction algorithm without stiffness estimation makes iterative corrections without accounting for the stiffness of the robot and the workpiece. In contrast, an interaction algorithm based on stiffness estimation can increase the normal force by a commanded amount ΔF_z while keeping the shear force F_x and torque T_y small. The stiffness estimation based algorithm is outlined in Algorithm 3.

Correction using stiffness: The stiffness matrix $\boldsymbol{K}$ is a map from the changes in the joint angles of the robot ($\Delta\theta_1, \Delta\theta_2, \Delta\theta_3$) to changes in the forces (ΔF_z, ΔF_x) and torque (ΔT_y) at the contact point. As given by,

$$\Delta\mathbf{F} = \boldsymbol{K}\ \Delta\boldsymbol{\Theta} = \boldsymbol{K}_p\ \Delta\mathbf{P}, \tag{4.4}$$

where $\Delta\mathbf{F} = \begin{bmatrix}\Delta F_z & \Delta F_x & \Delta T_y\end{bmatrix}^T$ and $\boldsymbol{K}_p \in \mathbb{R}^{3\times3}$ is the Cartesian stiffness matrix that maps displacements in the end-effector coordinate system $\begin{bmatrix}\Delta z & \Delta x & \Delta\theta_y\end{bmatrix}^T$ to the changes in contact point forces and torque $\Delta\mathbf{F}$, defined by Chen and Kao [28],

$$\boldsymbol{K}_p = \boldsymbol{J}(\boldsymbol{\theta})^{-T}(\boldsymbol{K}_\theta - \boldsymbol{K}_g)\boldsymbol{J}(\boldsymbol{\theta})^{-1}, \tag{4.5}$$

where $\boldsymbol{K}_\theta \in \mathbb{R}^{3\times3}$ is the joint stiffness matrix of the robot, $\boldsymbol{K}_g \in \mathbb{R}^{3\times3}$ is the complementary stiffness matrix arising from robot geometry changes due to external loading, and $\boldsymbol{J}(\boldsymbol{\theta}) \in \mathbb{R}^{3\times3}$ is the Jacobian matrix which maps the joint angle displacement $\Delta\boldsymbol{\Theta}$ to the end-effector displacements $\Delta\mathbf{P}$.

The stiffness matrix $\boldsymbol{K}$ is used to make corrective robot pose changes $\Delta\boldsymbol{\Theta}_d$ according to Eq. (4.4) for achieving a desired change in the forces and torque $\Delta\mathbf{F}_d$ to meet the objectives of the clamping operation, as,

$$\Delta\boldsymbol{\Theta}_d = \boldsymbol{K}^{-1}\Delta\mathbf{F}_d. \tag{4.6}$$

Algorithm 3 Interaction With Stiffness Estimation

Require: The tool is in contact with the tool guide as shown in Fig. 4.1 and the beam is unloaded.

Initialize:
Set target forces and torque: $\tilde{F}_z$, $\tilde{F}_x$ and $\tilde{T}_y$
Set normal force increment: $\Delta\tilde{F}_z$
Set normal force max (goal): $\tilde{F}_{z(max)}$
Set minimum joint move thresholds: $\Delta\theta_{min}$
Loop:
while $F_z < \tilde{F}_{z(max)}$ **do**
  if First Move
  for $i \in \{1, 2, 3\}$ **do**
    Move θ_i by $\Delta\theta_{min}$
    Record: F_z, T_y, F_x and θ_i
  end for then
    Calculate $\boldsymbol{K}_m$ as in Eq. (4.7)
  else
    Update the target normal force: $\tilde{F}_z + \Delta\tilde{F}_z$
    Calculate: $\Delta\boldsymbol{\Theta}$ using Eq. (4.9)
    for $i \in \{1, 2, 3\}$ **do**
      Move θ_i by $\Delta\theta_i$
      Record: F_z, T_y, F_x and θ_i
    end for
    Estimate $\boldsymbol{K}_m$ using Kalman Filter in Eq. (4.14) and Eq. (4.15)
  end if
  Loop:
  while $(|T_y| > \tilde{T}_y)$ *or* $(|F_x| > \tilde{F}_x)$ **do**
    Calculate: $\Delta\boldsymbol{\Theta}$ using Eq. (4.9)
    Move $\boldsymbol{\Theta}$ by $\Delta\boldsymbol{\Theta}$
  end while
end while

Measurement-based stiffness: The interaction stiffness $\boldsymbol{K}$ is directly estimated from measurements of forces and joint angles as $\boldsymbol{K}_m$,

$$\boldsymbol{K}_m = \begin{bmatrix} k_{\{F_z,\theta_1\}} & k_{\{F_z,\theta_2\}} & k_{\{F_z,\theta_3\}} \\ k_{\{F_x,\theta_1\}} & k_{\{F_x,\theta_2\}} & k_{\{F_x,\theta_3\}} \\ k_{\{T_y,\theta_1\}} & k_{\{T_y,\theta_2\}} & k_{\{T_y,\theta_3\}} \end{bmatrix}, \tag{4.7}$$

where each element $k_{\{F,\theta_i\}}$, with $F = \{F_z, F_x, T_y\}$ and $\theta_i \in \{\theta_1, \theta_2, \theta_3\}$, is defined as the ratio of the change in F (ΔF measured using force sensor) to a corresponding change in robot joint angle θ_i ($\Delta\theta_i$ obtained from robot joint encoders) as,

$$k_{\{F,\theta_i\}} = \frac{\Delta F}{\Delta \theta_i}. \tag{4.8}$$

The measured stiffness matrix $\boldsymbol{K}_m$ (a linear approximation of $\boldsymbol{K}$) can then be used to approximate the corrective robot pose changes in Eq. (4.6) using the measurement based $\Delta\boldsymbol{\Theta}_{d,m}$ computed as,

$$\Delta\boldsymbol{\Theta}_{d,m} = \boldsymbol{K}_m^{-1}\Delta\mathbf{F}_d \approx \Delta\boldsymbol{\Theta}_d. \tag{4.9}$$

However, uncertainty in the measurements of the forces and joint angles can lead to incorrect stiffness values $k_{\{F,\theta_i\}}$, which can in turn, cause large errors and rapid large changes in robot pose correction ($\Delta\boldsymbol{\Theta}_{d,m}$ in Eq. (4.9)). Nevertheless, the stiffness of the beam is expected to be continuous and change slowly for small motion of the robot. Therefore, a Kalman filter-based approach is used to smooth out the estimate of the individual elements of the stiffness matrix $\boldsymbol{K}_m$ in Eq. (4.9), similar to prior usage for constitutive parameter estimation in other applications, e.g., in [54].

Iterative stiffness estimation: The estimation of each element of stiffness matrix $\boldsymbol{K}_m$ in Eq. (4.7) as $\hat{k}_{\{F,\theta_i\}}$ at each iteration step t of the interaction algorithm is described below.

Step 1. Initialization: The variance $\sigma^2_{k_{\{F,\theta_i\}}}$ of the stiffness measurement $k_{\{F,\theta_i\}}$ in Eq. (4.8), for each element of $\boldsymbol{K}_m$ in Eq. (4.7), is obtained through initialization measurements using small robot motions in the initial pose of the robot, and is given in Table 4.1.

Table 4.1: Variances of $k_{\{F,\theta_i\}}$ in Eq. (4.8) obtained in the initialization step of the iterative stiffness estimation algorithm.

$\sigma^2_{k_{\{F,\theta_i\}}}$	θ_1	θ_2	θ_3
F_z	0.0034	0.0037	0.0032
F_x	0.1989	0.2850	0.2049
T_y	10^{-4}	10^{-4}	10^{-4}

Step 2. Prediction: In absence of an update equation for the stiffness in our model-free approach, the apriori estimate $\tilde{k}_{\{F,\theta_i\}}[t]$ of the stiffness is assumed to be the posteriori estimate $\hat{k}_{\{F,\theta_i\}}[t-1]$ at previous iteration step $t-1$,

$$\tilde{k}_{\{F,\theta_i\}}[t] = A\ \hat{k}_{\{F,\theta_i\}}[t-1], \tag{4.10}$$

where the gain $A = 1$. The apriori estimate of the variance in stiffness prediction $\tilde{P}_{k_{\{F,\theta_i\}}}[t]$ is taken to be the variance $\sigma^2_{k_{\{F,\theta_i\}}}$ obtained in the first iteration step (i.e. $t = 1$), and equal to the previous iteration's posteriori estimate of stiffness variance $\hat{P}_{k_{\{F,\theta_i\}}}[t]$ for $t > 1$,

$$\begin{aligned} \tilde{P}_{k_{\{F,\theta_i\}}}[t] &= \sigma^2_{k_{\{F,\theta_i\}}}, && t = 1, \\ &= \hat{P}_{k_{\{F,\theta_i\}}}[t-1], && t > 1. \end{aligned} \tag{4.11}$$

Step 3. Update: The apriori estimate $\tilde{k}_{\{F,\theta_i\}}[t]$ is updated to provide the posteriori estimate $\hat{k}_{\{F,\theta_i\}}[t]$ of the stiffness based on the force and encoder measurements at the current iteration. The predicted stiffness output, denoted as $\tilde{y}[t]$, is modeled as a random walk from the apriori stiffness estimate $\tilde{k}_{\{F,\theta_i\}}[t]$, similar to the approach in [**?**],

$$\tilde{y}[t] = C\tilde{k}_{\{F,\theta_i\}}[t] + Q \tag{4.12}$$

with the measurement gain $C = 1$ and the measurement variance is taken to be $Q = \sigma^2_{k_{\{F,\theta_i\}}}$ obtained from the initialization step. The actual stiffness output at current iteration step $y[t]$ is found from sensor measurements as,

$$y[t] = \frac{\Delta F[t]}{\Delta \theta_i[t]}, \tag{4.13}$$

where $\Delta F[t] = F[t] - F[t-1]$ and $\Delta\theta_i[t] = \theta_i[t] - \theta_i[t-1]$ are the changes in the force and joint angle measurements at the current iteration step t compared to the previous iteration step $t-1$. The posteriori estimate of the stiffness $\hat{k}_{\{F,\theta_i\}}$ and stiffness variance $\hat{P}_{\{F,\theta_i\}}$ is then obtained using as,

$$\hat{k}_{\{F,\theta_i\}}[t] = \tilde{k}_{\{F,\theta_i\}} + \alpha[t]e_y[t], \tag{4.14}$$

$$\hat{P}_{\{F,\theta_i\}}[t] = (1 - \alpha[t])\tilde{P}_{\{F,\theta_i\}}[t], \tag{4.15}$$

where $e_y[t]$ is the innovation error, defined as the difference between the actual output $y[t]$ and the predicted output $\tilde{y}[t]$ computed as,

$$e_y[t] = y[t] - \tilde{y}[t], \tag{4.16}$$

and $\alpha[t]$ is the Kalman gain,

$$\alpha[t] = \tilde{P}_{\{F,\theta_i\}}[t] \ \Big(\ \tilde{P}_{\{F,\theta_i\}}[t] \ + Q \Big)^{-1}. \tag{4.17}$$

4.2 Results and Discussion

In the following, results of the interaction algorithm without stiffness estimation are evaluated against the proposed approach with stiffness estimation.

4.2.1 Stiffness estimation reduces number of iterations

The number of iterations N_i is the total number of position-adjustment steps the robot takes to reach the required normal force of $F_z = 10N$ while maintaining small shear force $|F_x| < \tilde{F}_x$ and torque $|T_y| < \tilde{T}_y$. Additionally, the normal force increment ΔF_z is the change in normal force each time the robot moves forward, whether it results from an incremental movement as in Algorithm 2 or a commanded change in force as in Algorithm 3. From Fig. 4.3, the interaction algorithm with stiffness estimation completes the task with approximately four times fewer iterations as compared to the approach without stiffness estimation. For example, as shown by results from one of the trials with normal force increment $\Delta F_z \approx 1N$ shown in Fig. 4.4 for the approach without stiffness estimation, the number of iterations taken to complete the task is $N_i = 48$. In comparison, the number of iterations with stiffness estimation is $N_i = 11$ for approximately the same normal force increment $\Delta F_z = 1N$ as shown in Fig. 4.5. Thus, with stiffness estimation, the operating speed is approximately four times faster when compared to the approach without stiffness estimation. Details of results are shown in Table 4.2.

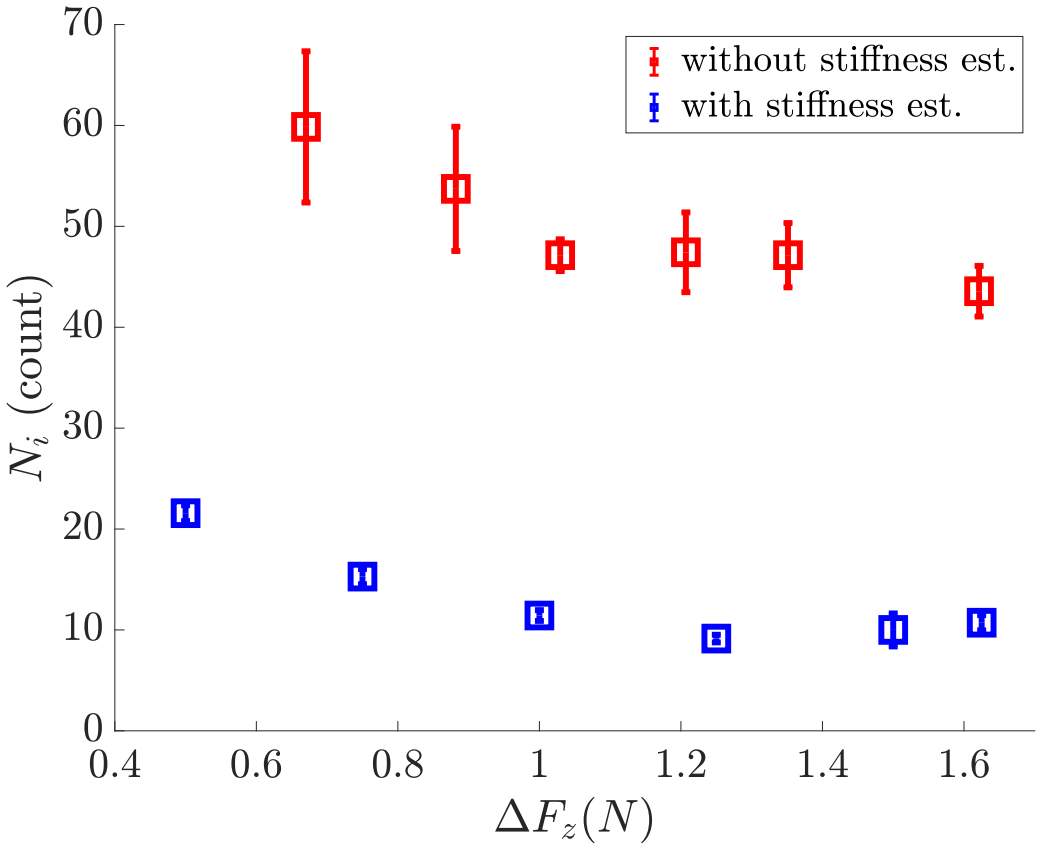

Figure 4.3: The average number of iterations N_i over 7 trials is compared at a target normal force of $\tilde{F}_z = 10N$, with and without stiffness estimation, for 6 different normal force increments ΔF_z. The number of iteration are lower by approximately 65% for the approach with stiffness estimation as compared to the case without it.

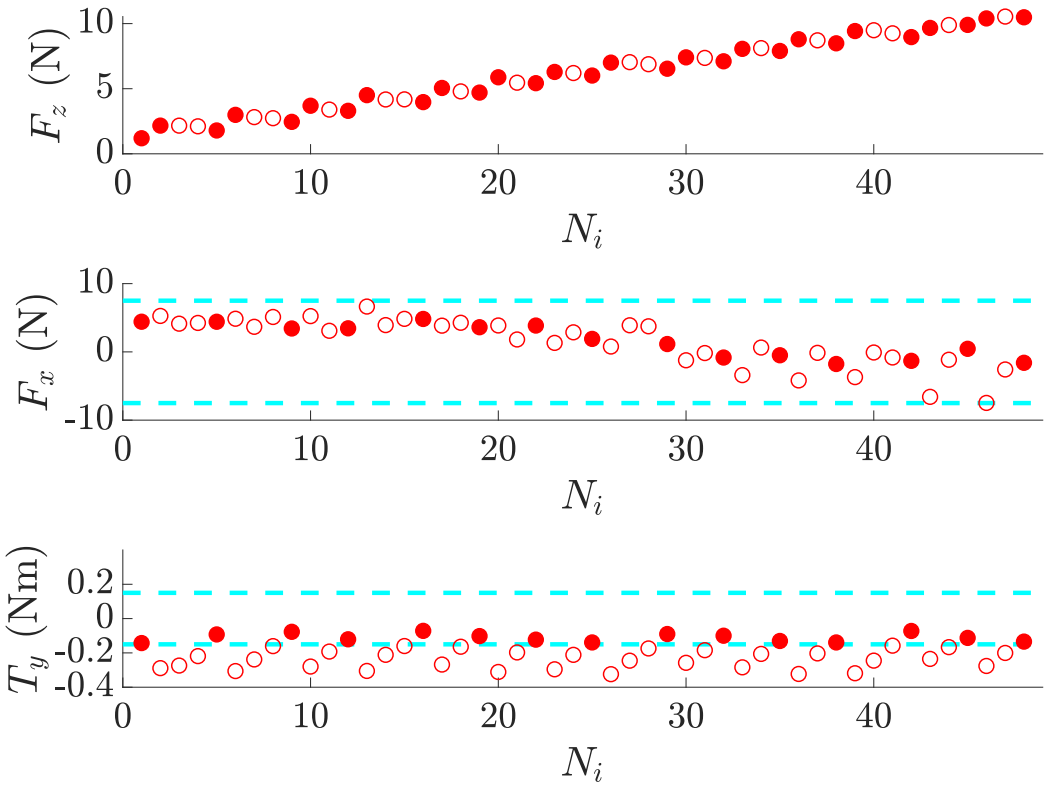

Figure 4.4: Measured interaction forces and torque without stiffness estimation for an increment in normal force $\Delta F_z \approx 1N$, selected (closest to the mean) from the seven trials shown in Table 4.2. The solid red circles indicate when the robot can be incremented forward as the torque and shear force have become sufficiently small (inside threshold values indicated by the cyan dashed lines). In general, there are two to three correction iterations present, indicated by the empty circles between the forward increments.

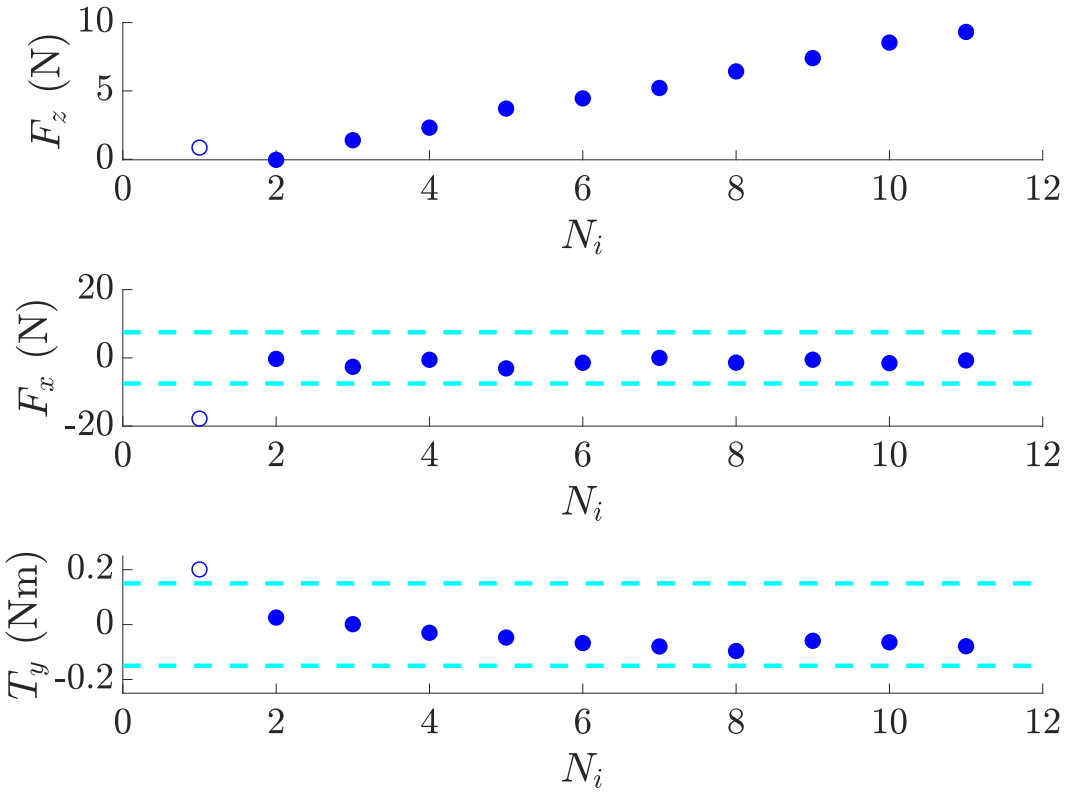

Figure 4.5: Measured interaction forces and torque with stiffness estimation and a normal-force increment $\Delta F_z = 1N$, selected (closest to the mean) from the seven trials shown in Table 4.2. The solid blue circles indicate when the robot's normal force can be incremented forward as the torque and shear force have become sufficiently small (inside threshold values indicated by cyan dash lines). In this case there is only one correction iteration indicated by the empty circles.

4.2.2 Stiffness estimation reduces correction steps

Number of correction steps N_c is the number of motions the robot takes to reduce shear force F_x and torque T_y to stay within the corresponding threshold values $\tilde{F}_x = \pm 7.5N$ and $\tilde{T}_y = \pm 0.15Nm$. The interaction algorithm without stiffness estimation requires several correction steps to keep the shear force F_x and torque T_y within the threshold. Typically, 60% to 80% of the total number of iterations N_i are correction steps N_c needed to complete the task, as shown in Fig. 4.6 and Table 4.2. This is because without any stiffness estimation, the robot only relies on an iterative position correction with fixed predefined steps. Therefore, if shear force and torque are large, then it can take two or more steps to correct after each increase of the normal force ΔF_z.

The percentage of correction steps N_c reduces substantially, ranging from 5% to 30% with stiffness estimation as shown in Fig. 4.6 and Table 4.2. Typically, after the initial assessment the robot can correct for large shear force and torque in one step and remains within the threshold until the task is completed. Thus, by using the estimated stiffness from measurement, the robot is able to predict its next pose in a single step.

A comparison can be made from the results shown in Figs. 4.4 (without stiffness estimation) and 4.5 (with stiffness estimation). The approach without stiffness estimation requires multiple corrections (two to three) between forward increments in normal force ΔF_z. Alternatively, the interaction with stiffness estimation only requires one step of correction to minimize shear force F_x and torque T_y at the beginning of the operation. Thus, the algorithm with data-based stiffness estimation leads to a substantial reduction of the correction steps.

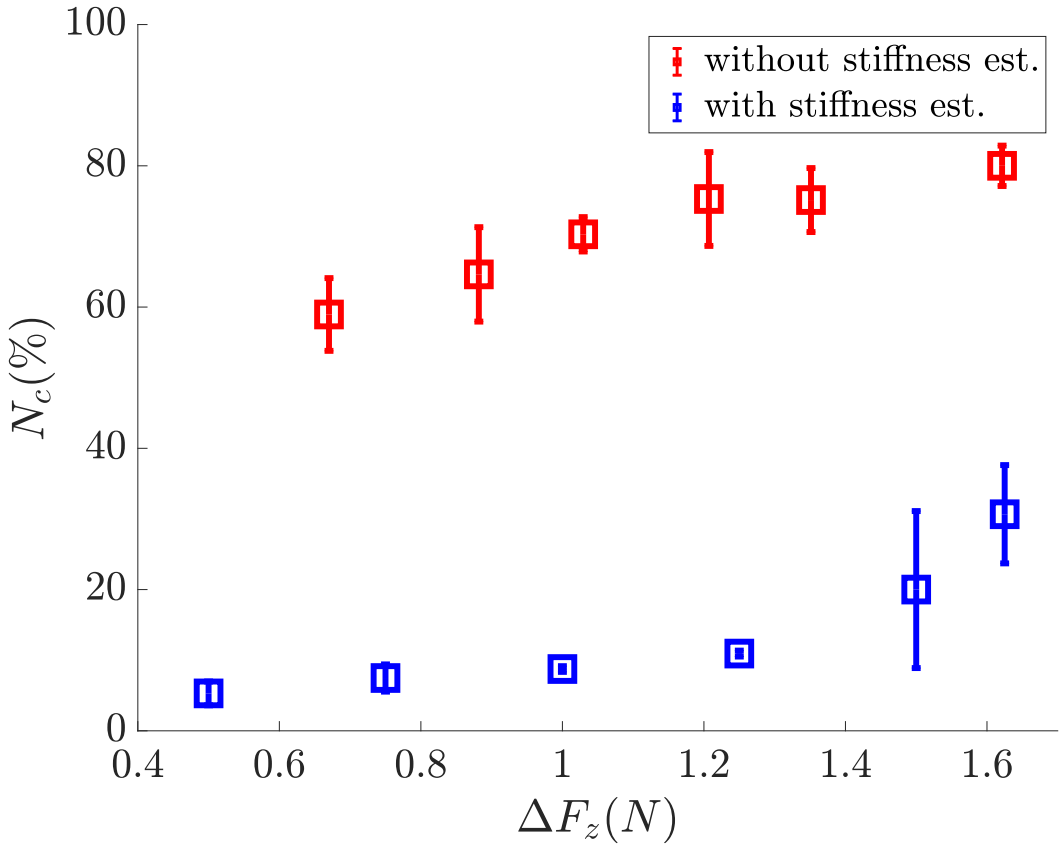

Figure 4.6: The average percentage of correction steps N_c (of the total iterations N_i) taken to minimize shear force F_x and torque T_y over 7 trials is compared, with and without stiffness estimation, for 6 different normal force increments ΔF_z. Typically, the approach with stiffness estimation only needs a few correction to maintain acceptable shear force and torque as compared to the approach without it.

Table 4.2: Comparative results, with and without stiffness estimation: number of iterations N_i and percentage of correction steps N_c (of the total iterations N_i). The experiment was performed seven times for several different normal force increment ΔF_z and mean μ and standard deviation σ for each metric is presented over seven trials.

	$\Delta F_z(N)$ $\mu \pm \sigma$	N_i(count) $\mu \pm \sigma$	$N_c(\%)$ $\mu \pm \sigma$
	0.67 ± 0.09	59.85 ± 7.49	58.95 ± 5.15
Without	0.88 ± 0.09	53.71 ± 6.15	64.62 ± 6.68
Stiffness	1.03 ± 0.03	47.42 ± 3.95	75.30 ± 6.64
Estimation	1.20 ± 0.10	47.14 ± 3.18	75.15 ± 4.52
	1.35 ± 0.06	43.57 ± 2.50	80.00 ± 2.85
	1.62 ± 0.06	47.14 ± 1.57	70.30 ± 2.43
	0.5	21.00 ± 0.78	5.30 ± 1.68
With	0.75	15.28 ± 0.75	7.47 ± 1.92
Stiffness	1.00	11.42 ± 0.53	8.75 ± 0.40
Estimation	1.25	9.14 ± 0.37	10.93 ± 0.42
	1.50	10.00 ± 1.63	20.00 ± 11.11
	1.62	10.71 ± 0.75	30.67 ± 6.95

4.3 Chapter Conclusions

This work developed and evaluated a model-free data-based method for robotic interactions with flexible structures to account for the elasticity of the robot and workpiece. The method does not require prior knowledge of the system such as the robot kinematics or robot-workpiece stiffness. Furthermore, the experimental results show that the learned data-based method, with estimated stiffness, can be used to substantially increase the operation speed by four times.

Chapter 5

ACTIVE DATA-ENABLED ROBOT LEARNING OF ELASTIC WORKPIECE INTERACTIONS

This chapter addresses the main contribution **MC2**; *With a minimum number of known measurement locations efficiently predict controlled interactions at unmeasured locations*, and has been submitted for publication as a journal article [3]. The main contributions of this chapter are: (i) to use Gaussian Process methods to learn the robot pose for force normality at unmeasured workpiece locations; and (ii) to use active learning for optimally selecting and minimizing the number of measurement locations needed for accurate learning of the robot-pose map with the data-enabled approach.

The rest of this chapter is organized as follows. A description of the experiment, with proposed active learning of the robot pose map is presented in Section 5.1. Results and discussion of the experiment are presented in Section 5.2. Lastly, conclusions are presented in Section 5.3.

5.1 Methods

The robot-workpiece interaction explored in this paper characterizes a robotic clamping operation with an elastic workpiece. This robotic interaction is challenging because the robot pose can change substantially during the process due to large deflection of the workpiece as shown in Fig. 5.1. Additionally, the clamping operation can vary significantly by changing the interaction position along the workpiece, as workpiece stiffness and robot pose change.

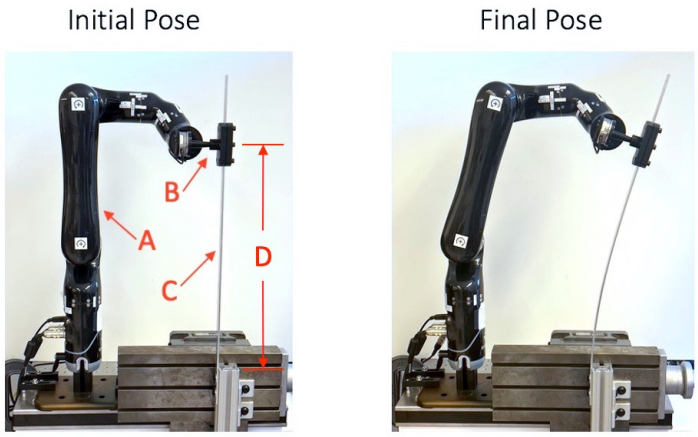

Figure 5.1: Experimental setup: (Left) The Kinova MICO robot (A) applies force through a tool (B) onto a flexible aluminum beam (C) which is shown in the undeformed configuration. The distance between the beam's mounting point and the tool's contact point (D) can vary from 315 mm to 415 mm. (Right) The applied normal force can lead to significant deflection of the flexible beam.

5.1.1 Experimental Setup

The experimental setup illustrated in Fig. 5.1, includes a Kinova MICO robotic arm with an ATI Mini 45 six degrees of freedom Force-Torque (F/T) sensor mounted on the end-effector. The robot's end-effector is securely connected to a flexible beam using a 3D-printed tool and tool guide illustrate in Fig. 5.2. The distance D in Fig. 5.1 from the beam mounting point to the tool contact point can range from 315 mm to 415 mm by adjusting the tool guide position on the beam. The beam is constructed from 6061-T6 aluminum with a width of 18.9 mm and a thickness of 3.15 mm.

The clamping operation requires operating the robot such that a prescribed normal contact force F_z is applied to the beam, while normality is maintained between the Tool and the Tool Guide (see Fig. 5.2) in order to avoid tool and/or workpiece damage. The normality is defined as the bounded shear force $F_x < |\tilde{F}_x|$ and torque $T_y < |\tilde{T}_y|$ throughout the oper-

ation, which are measured by the F/T sensor. Additionally it is assumed that as the beam deflection increases through the clamping operation, the corresponding normal force F_z in Fig. 5.2 will also increase.

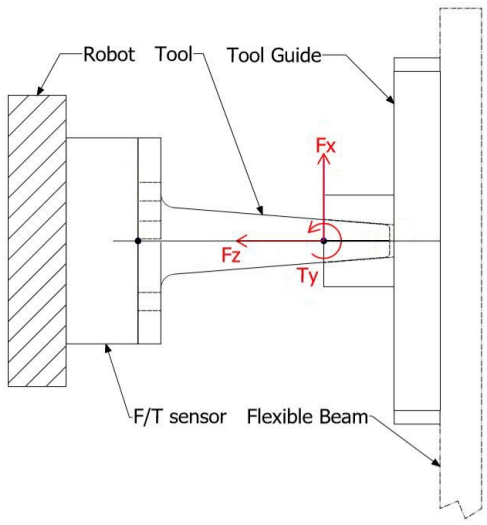

Figure 5.2: Diagram of the tool contact point. The aim is to increase the normal force F_z to a predetermined level, while simultaneously minimizing the shear force F_x and torque T_y at the contact point to prevent any potential damage to the tool or workpiece. These forces are measured with a force-torque (F/T) sensor in the coordinate frame of the tool contact point as shown in red.

5.1.2 Current Stiffness-based Robot-pose Estimation

The normal force F_z between the tool and workpiece is increased incrementally by moving the robot towards the workpiece along the tool axis by Δz, producing a change in normal force ΔF_z as illustrated in Fig. 5.2, where the the Force/Torque (F/T) sensor is placed between the robotic arm and the tool. As the robot moves forward in the **z** direction at each increment, the shear force and torque at the contact point between the tool and the workpiece can change since the tool does not necessarily remain normal to the workpiece

surface due to the additional deflection of the workpiece. The robot corrects for the change in shear force and torque by moving the tool tip in the **x** direction and rotating around the **y**-axis, in an iterative manner. The robot-pose correction can be found using estimated robot-workpiece stiffness (from data), [2]. For example, the local change $\Delta\mathbf{F}$ (ΔF_z, ΔF_y and ΔT_x) in applied forces and torques between the tool and the workpiece can be related to change $\Delta\mathbf{\Theta}$ ($\Delta\theta_1$, $\Delta\theta_2$ and $\Delta\theta_3$) in the robot pose (Fig. 5.3) through the local stiffness $\mathbf{K}(F_z, X_w)$ that depends on the location X_w of the applied force on the workpiece and the magnitude of the applied normal force F_z, [2, 28]

$$\Delta\mathbf{F} = \mathbf{K}(F_z, X_w)\, \Delta\mathbf{\Theta}. \tag{5.1}$$

The local stiffness $\mathbf{K}$ includes the effects of both (i) the workpiece stiffness and (ii) the robot stiffness at the selected robot pose, and can be estimated from measurements of the change $\Delta\mathbf{F}$ in applied forces and torques and robot pose change $\Delta\mathbf{\Theta}$. Corrective robot pose changes $\Delta\mathbf{\Theta}_d$ can be found from Eq. (5.1) for achieving a desired change in the forces and torque $\Delta\mathbf{F}_d$, as

$$\Delta\mathbf{\Theta}_d = \mathbf{K}^{-1}\Delta\mathbf{F}_d. \tag{5.2}$$

Once the tool tip shear force and torque are within the desired thresholds of $F_x < |\tilde{F}_x| = 7.5$ N and torque $T_y < |\tilde{T}_y| = 0.15$ Nm. The incremental displacement along the **z**-axis continues until the measured normal force F_z reaches the required maximum normal force $\tilde{F}_z = 10$ N and the shear force F_x and the torque T_y are below the required thresholds. At every step in the process the forces and torques, F_z, F_x and T_y as well as robot joint angles θ_1, θ_2 and θ_3 are measured and recorded at the specific workpiece location X_w. As a result, one obtains measurements of the robot pose map $\mathbf{\Theta}(F_z, X_w)$ as a function of the normal force F_z at the same specified location X_w.

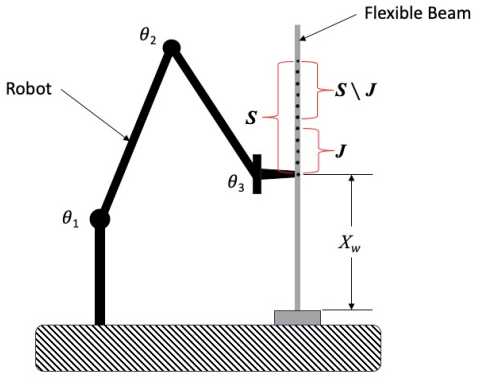

Figure 5.3: Research problem. The goal is to learn the robot-pose map $\boldsymbol{\Theta}(F_z, X_w)$ comprising of joint angles $(\theta_1, \theta_2, \theta_3)$ that result in a prescribed normal force F_z, while ensuring small shear force F_x and torque T_y, as in Fig. 5.2 at all $\boldsymbol{S}$ potential work locations points X_w. Given prior measurements $\boldsymbol{J}$ at some locations, the active learning approach seeks to select the optimal measurement point in the unexplored region $\boldsymbol{S} \setminus \boldsymbol{J}$.

5.1.3 Problem Statement

The existing method uses measured data to iteratively adjust robot-workpiece alignment as the normal force is increased in slight increments while force normality ($F_x < |\tilde{F}_x|$ and $T_y < |\tilde{T}_y|$) is maintained. This process yields the robot pose map $\boldsymbol{\Theta}(F_z, X_w)$, essential for attaining a specified normal force F_z at a designated location X_w on the workpiece. It's important to note that the set $\boldsymbol{S}$ of potential workpiece locations is finite and the iterative procedure must be repeated for each location $X_w \in \boldsymbol{S}$ on the workpiece.

The research objective is to enhance the overall robot-workpiece interaction efficiency by limiting the iterative process to only the necessary locations $\boldsymbol{J} \in \boldsymbol{S}$. This approach speeds up the overall process of learning the robot pose map $\boldsymbol{\Theta}(F_z, X_w)$ from a minimal set of specified normal forces F_z and measurement locations X_w on the workpiece, leading to robot joint

angles represented as:

$$\begin{bmatrix} \theta_1 \\ \theta_2 \\ \theta_3 \end{bmatrix} = \boldsymbol{\Theta}(F_z, X_w). \tag{5.3}$$

Specifically, this is an Active Learning problem that endeavors to best select the next measurement location in the unexplored region of the workpiece based on the given J prior measurements. Subsequently, the learned robot pose map $\boldsymbol{\Theta}(F_z, X_w)$ enables the inference of the robot pose, (θ_1, θ_2, θ_3) required to attain the desired normal forces F_z at new locations X_w without the need for the iterative procedure.

5.1.4 Proposed Active Learning of the Robot Pose Map

The robot pose needed to achieve the desired normal force at different locations can be learned using regressions techniques from the prior measurements on the workpiece, [52]. Briefly, each robot joint angle θ_i ($i = 1, 2, 3$) can be considered as a zero-mean real-valued Gaussian process (GP) over the input space $W = [F_z, X_w^T]^T$

$$\theta_i(W) \sim GP\left(0, \tilde{k}(W, W')\right) \tag{5.4}$$

with covariance $\tilde{k}(W, W')$, and measurements given by $\theta_{i,m} = \theta_i(W) + \epsilon$, where ϵ is an additive, zero-mean, independent identically distributed Gaussian noise with variance σ^2, i.e., $\epsilon \sim \mathcal{N}(0, \sigma^2)$. Then, the prediction $\theta_\star$ at W (new location and normal force), given M measured data

$$\boldsymbol{\theta}_{i,m} = \begin{bmatrix} \theta_{i,m_1} & \theta_{i,m_2} & \dots & \theta_{i,M} \end{bmatrix}^T \tag{5.5}$$

at inputs $\mathbf{W} = [W_1\ W_2\ \ldots\ W_M]$, is Gaussian, i.e., $\theta_\star|\mathbf{W}, \mathbf{y}, W \sim \mathcal{N}\left(\bar{\theta}_\star, \sigma^2_{\theta_\star}\right)$, given by [52]

$$\bar{\theta}_\star(W) \quad = K(W, \mathbf{W}) \left[K(\mathbf{W}, \mathbf{W}) + \sigma^2 I\right]^{-1} \boldsymbol{\theta}_{i,m} \tag{5.6}$$

$$\sigma^2_{\theta_\star}(W) = K(W, W) - K(W, \mathbf{W}) \left[K(\mathbf{W}, \mathbf{W}) + \sigma^2 I\right]^{-1} K(\mathbf{W}, W) \tag{5.7}$$

with $K(\mathbf{W}, W)$ denoting the covariances evaluated at all pairs of measured input $\mathbf{W}$ and the prediction input (location, normal force) W, and the other covariance matrices $K(\cdot, \cdot)$ are defined similarly.

We assume that we are free to choose the order of opperations at the J measurement locations on the workpiece. Then the sequence $X_{w,j}$ can be selected to speed up the learning of the pose map $\boldsymbol{\Theta}(X_w, F_z)$. Active learning endeavors to minimize the effort of collecting/labeling training data while ensuring model prediction accuracy, especially in scenarios where the labeling cost cannot be ignored, [55]. One approach is to use Bayesian optimal design of experiments to improve the expected information gain, i.e., maximizing the information gain (the KL divergence between the current estimation and the hypothetical next-step estimation), e.g., [56], of the pose map $\boldsymbol{\Theta}(X_w, F_z)$. However, the clamping and unclamping operation takes a significant amount of time compared to the time needed to make measurements all the variations of the normal force F_z for each specified work location $X_{w,j}$. Hence it is more efficient to collect all the normal force measurements at each work location, and the active learning objective is modified to the just the optimal selection of the next measurement location $X_{w,J+1}$ after J sets of measurement locations. A modified approach, based on the uncertainty (δ) sampling method [57], is proposed here to select the next measurement location $X_{w,J+1}$ by maximizing the accumulated variance of all joint angle predictions for the desired normal force F_z at the unexplored locations $X_{w,u} \in S_{u,J} \triangleq \boldsymbol{S} \setminus S_J$ on the workpiece with $S_{u,J} = \{X_{w,j}\}_{j=1}^{J}$ being the set of already explored measurement

locations, i.e.,

$$\begin{aligned} X_{w,J+1} &= \text{argmax}_{X_{w,u}\in S_{u,J}} \sum_{k=0}^{K}\sum_{i=1}^{3} \sigma^2[\theta_i(k\Delta F_n, X_{w,u})] \\ &= \text{argmax}_{X_{w,u}\in S_{u,J}} \delta(X_{w,u}) \\ &= \text{argmax}_{X_{w,u}\in S_{u,J}} \text{trace}(\Sigma_u), \end{aligned} \tag{5.8}$$

the steps of which are summarized in Algorithm 4. Here we are minimizing the trace of the covariance matrix Σ_u, which maximizes the sum of the output variances σ^2 of the GPs, [58].

Note that the element at the i^{th} row and j^{th} column of the covariance matrix $\Sigma_u \in \mathbb{R}^{3(K+1)\times 3(K+1)}$ describes the correlation between the random variable $\theta_p(p_0\Delta F_n, X_{w,n})$ and $\theta_q(q_0\Delta F_n, X_{w,n})$ where p, q are given by the index maps

$$p = \text{idxMap}(i), q = \text{idxMap}(j) \tag{5.9}$$

with $\text{idxMap}(s) = \max(0, s-1)/(K+1) + 1$ (integer division), and p_0, q_0 are given by the index force maps

$$p_0 = \text{idxMap}_F(i), q_0 = \text{idxMap}_F(j) \tag{5.10}$$

with $\text{idxMap}_F(s) = \text{mod}(s-1, K+1)$. The maximum predicted standard deviation $\overline{\sigma}$ among the unexplored work locations

$$\overline{\sigma} = \max_{X_{w,u}\in S_{u,J}, i\in[1,3], k\in[0,K]} \sigma[\theta_i(k\Delta F_n, X_{w,u})] \tag{5.11}$$

is used here to describe the uncertainty variation when more training data is collected, i.e., as the number of total measurement locations J increases.

In this application the set of manufacturing locations was discrete. For an unexplored

Algorithm 4 Active Data-enabled Learning of the pose map $\boldsymbol{\Theta}$

Require: unexplored set $S_{u,0} = \boldsymbol{S}$, required normal force $\tilde{F}_z$ and the normal force increment ΔF_z, maximum standard deviation $\overline{\sigma} = +\infty$, standard deviation threshold ϵ, allowed maximum number of measurements M, training set $S_{ts} = \{\}$, robot pose map $\boldsymbol{\Theta}(F_z, X_w)$ comprising of GPs for joint angles $\theta_i(F_z, X_w)$ $(1 \leq i \leq 3)$.

1: **Initialize**$(J = 1)$:
2: Set the robot to the initial pose as in Fig. 5.3 with interaction point $X_{w,1}$ and collect $S_n = \{F_{z,n}, X_{w,1}, \boldsymbol{\theta}_1, \boldsymbol{\theta}_2, \boldsymbol{\theta}_3\}$ by the method in Section 5.1.2.
3: Update the unexplored set $S_{u,1}$.
4: **while** $J < M$ and $\overline{\sigma} > \epsilon$ **do**
5: $S_{ts} \leftarrow S_{ts} \bigcup S_n$.
6: Train the models $\theta_i(\cdot)$ with training set S_{ts}.
7: Update the maximum standard deviation $\overline{\sigma}$ using Eq. (5.11).
8: Obtain the next work location $X_{w,J+1}$ for collecting training data by maximizing the accumulated variance as in Eq. (5.8).
9: Repeat line 2 with the selected location $X_{w,J+1}$ and corresponding initial pose.
10: Update the unexplored set $S_{u,J+1}$ by removing the $X_{w,J+1}$ from the set $S_{u,J}$.
11: $J \leftarrow J + 1$.
12: **end while**
13: **return** the learned robot pose map $\boldsymbol{\Theta}(F_z, X_w)$.

set that covers a continuous space, gradient-based or Bayesian optimization methods, [59], can be used to find the next clamping location $X_{w,J+1}$ in line 8 of Algorithm 4.

5.1.5 Linear Positioning Learning of the Robot Pose Map

In contrast to the Active Learning approach discussed in in Section 5.1.4, Linear Positioning Learning of the robot-pose map $\boldsymbol{\Theta}(F_z, X_w)$ is also explored, as a benchmark to compare against. Specifically, the tool is moved across the unexplored region of the beam as shown in Fig. 5.3, from one end $X_{w,1}$ to the other with a constant increment ΔX_w, i.e., the procedure is the same as Algorithm 4 but with the active learning at line 8 replaced with selecting the next location by adding 10 mm to the previous location $X_{w,J+1} = X_{w,J} + \Delta X_w$. It is noted that for manufacturing process such as clamping and drilling, the Linear Positioning

Learning with incremental change of the tool position X_w relative to the workpiece is a reasonable procedure as it minimizes re-positioning efforts, [60, 61].

5.1.6 Rapid Robot-Workpiece Elastic Interactions

Once the robot-pose map $\boldsymbol{\Theta}(F_z, X_w)$ has been learned, it can be used to increased process efficiency. Predicted robot-workpiece interactions can be used to rapidly increase the normal force F_z at unexplored locations X_w on the workpiece. The predicted robot-workpiece interactions at unexplored locations, are reproduced at faster speeds by the same process used in [1] at the prior measurement locations (as opposed to unexplored locations in this article). The learned robot-pose map $\boldsymbol{\Theta}(F_z, X_w)$ is used to generate the required robot joint velocity trajectories as it provides the necessary relationship between the normal force F_z, measurement location X_w and joint angles θ_i from Eq. (5.3). This allows for robot joint velocities trajectories to be created that can accommodate any specified time-based normal-force profile and workpiece location.

5.2 Results and Discussion

Comparisons are made between the two methods (proposed Active Learning in Section 5.1.4 and Linear Positioning Learning in Section 5.1.5) to show the efficacy of active learning in terms of the number of total experiments and the resultant ability to rapidly control the Robot-Workpiece elastic interactions at the unmeasured locations.

In the experiment, following Algorithm 4, the set of measurement locations $\boldsymbol{S}$ consists of 11 evenly spaced locations from 315 mm to 415 mm, i.e., $\{X_w\} \in [315 \text{ mm}, 415 \text{ mm}]$ at 10 mm increments. Therefore, the constant increment ΔX_w in the Linear Positioning Learning in Section 5.1.5 is set to $\Delta X_w = 10$ mm. The required normal force $\tilde{F}_z = 10$ N and the normal force incremental $\Delta F_n = 0.5$ N. The allowed number of measurements $M = 11$ and

the standard deviation deviation threshold $\epsilon = 0.01$ rad is selected because the variation ϵ in the joint angles θ_i will break the normality.

5.2.1 Active Learning Requires Less Training.

Gaussian Process Regression methods with Active Learning requires less training compared to the Linear Positioning Learning. The plot of the maximum standard deviation $\overline{\sigma}$ with respect to the number of measurement locations J is shown in Fig. 5.4. The total number of J measurement operations needed to reach the threshold ϵ value for the maximum predicted standard deviation $\overline{\sigma}$ from Eq. (5.11), is an indication of how well each learning process is preforming. After $J = 2$ set of measurements, the maximum standard deviation $\overline{\sigma}$ in Active Learning process has reached a value of $\overline{\sigma} = 0.01$ rad $\leq \epsilon = 0.01$ rad and become flat. In contrast, the Linear Positioning method does not achieve a similar state of $\overline{\sigma} = 0.01$ rad until $J = 9$ measurement locations have been completed. The number of measurements needed with Active Learning is 77.8% less than the case without Active Learning to achieve a similar level of model precision. Moreover, with an equal number of acquired set of measurements ($J = 2$), the Active Learning process yields a maximum predicted standard deviation of $\overline{\sigma} = 0.01$ rad, while without Active Learning, the standard deviation is $\overline{\sigma} = 0.41$ rad. This implies a notable 97.6% improvement in the maximum predicted standard deviation when Active Learning is employed given the same number of measurement locations $J = 2$.

It is noted that the rate of learning can be improved using heuristics when compared to the Linear Positioning learning if there is apriori knowledge of the part's stiffness variations. For the current beam example, one expects the structure stiffness to decrease continuously as the robot moves towards the free end of the beam. Therefore, in this case, where the work locations are arranged in a linear manner, a binary-search-type approach can lead to improved learning compared to the Linear Positioning learning. The proposed Active Learning

process leads to a training sequence which is close to a binary search, but it infers this in a systematic manner from the measured data without the use of apriori knowledge about the elastic interactions. Moreover, the Active Learning process is applicable in more complex settings, without apriori knowledge of the combined robot-structure stiffness variations over the set of work locations.

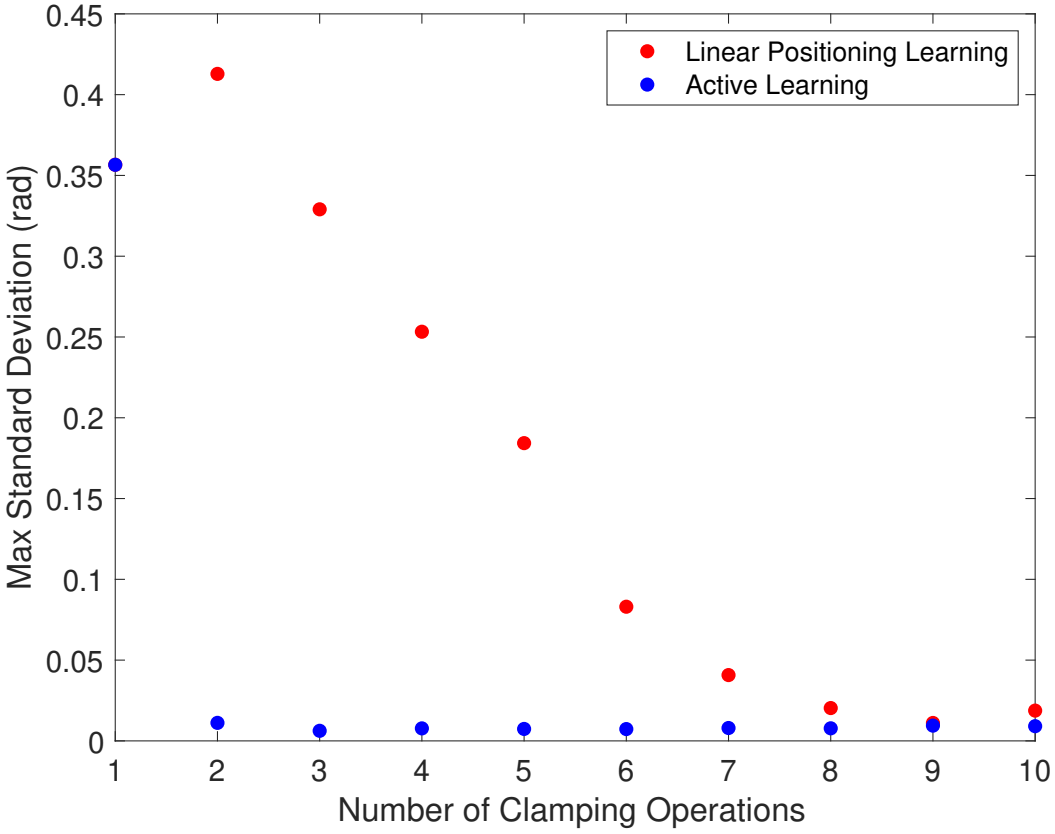

Figure 5.4: Maximum standard deviation $\overline{\sigma}$ for predicted robot joint angles in the unexplored region of the workpiece as in Eq. (5.11) after J sets of measurements for training.

Table 5.1: Sequence of location selections $\{X_{w,j}\}_{j=1}^{j=11}$ by Linear Positioning Learning (LPL) and Active Learning (AL).

j	LPL	AL	j	LPL	AL
$X_{w,1}$	315	315	$X_{w,7}$	375	325
$X_{w,2}$	325	415	$X_{w,8}$	385	355
$X_{w,3}$	335	365	$X_{w,9}$	395	395
$X_{w,4}$	345	385	$X_{w,10}$	405	345
$X_{w,5}$	355	335	$X_{w,11}$	415	375
$X_{w,6}$	365	405			

5.2.2 Force Normality at Unmeasured Locations

Gaussian Process Regression methods in conjunction with Active Learning enables the effective learning of the robot pose map $\mathbf{\Theta}(F_z, X_w)$ to ensure force normality in areas of the workpiece that are not directly measured. After $J = 4$ measurement locations in the Active Learning process, the maximum standard deviation $\overline{\sigma}$ has reduced to value of $\overline{\sigma} \approx 0.008$ rad for the remaining unmeasured workpiece locations. In contrast, the Linear Learning process yields a value of $\overline{\sigma} = 0.253$ rad and continues to decrease substantially with further sets of measurements, as can be seen in Fig 5.4. After $J = 4$ measurements the Linear Learning process is selecting a workpiece location of $X_w = 355$ mm for the next measurement location $X_{w,5}$ as can be seen by the sequence of locations selected by each process in Table 5.1. This workpiece location of 355 mm is used for a direct comparison of the ability of the GPR predicted robot pose maps to achieve force normality under robot-workpiece interactions for both the Active and Linear Learning processes.

Using GPR training sets $S_{t,s}$ selected by both the Linear and Active process, each containing $J = 4$ measurement locations, predicted robot-workpiece interactions are conducted at a workpiece location of 355 mm and at the same speed as the measurement process used during training, taking 93 seconds. The prescribed sigmoidal normal force F_z profile for the

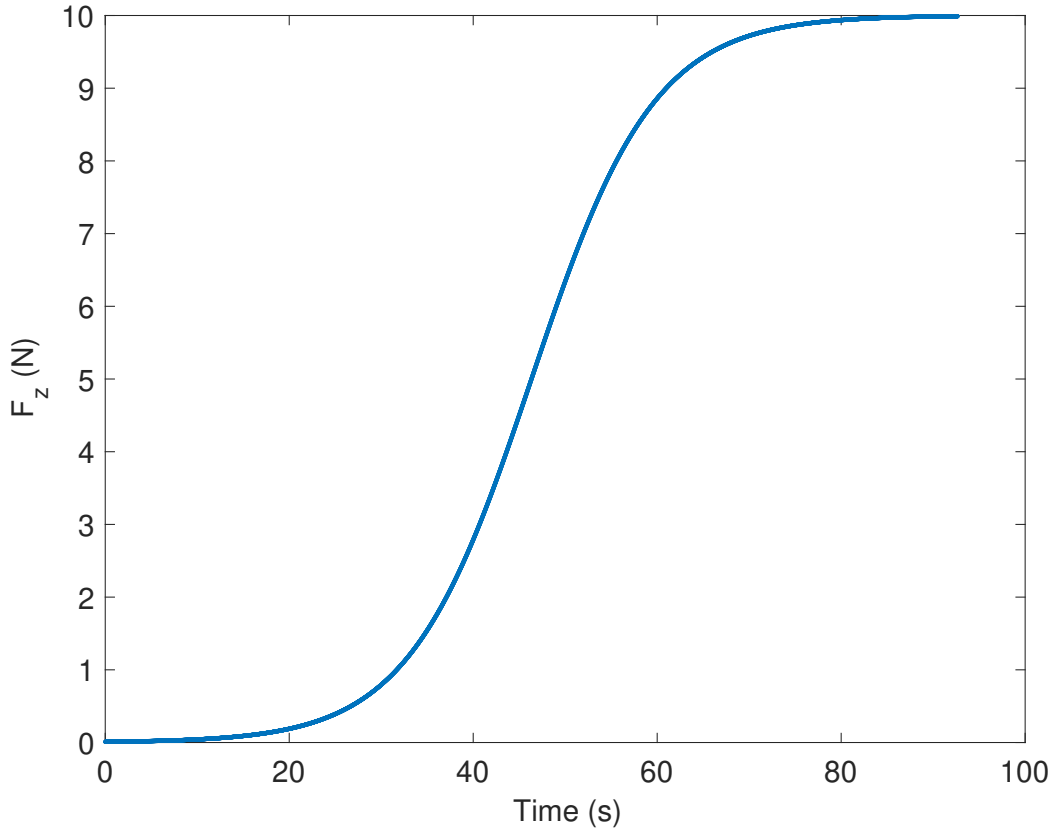

Figure 5.5: The prescribed sigmoidal normal force F_z profile used at workpiece location $X_w = 355$ mm to predict joint angles in Fig. 5.6 with the robot pose map $\mathbf{\Theta}(F_z, X_w)$.

predicted robot-workpiece interactions can be seen in Fig. 5.5, this is used with the pose map $\mathbf{\Theta}(F_z, X_w)$ to to predict robot joint angles for the workpiece location of 355 mm as seen in Fig. 5.6. Results from the predicted robot-workpiece interactions can be seen for the the Linear process and Active process in Fig. 5.7. For the predicted interactions, acceptable ranges for the shear force F_x and the torque T_y are set to be two times the corresponding positioning-error-based thresholds (the ultimate accuracy of the robot) from the robot-pose estimation process in Section 5.1.2, $|F_x| < 15$ N and $|T_y| < 0.3$ Nm, respectively. By com-

paring Fig. 5.7(a) and Fig. 5.7(b) it can be seen that the robot pose map trained with Active Learning can effectively predict the joint angles and desired normal force profile needed for the robot-beam interaction at the unexplored workpiece location of 355 mm but the Linear Positioning Learning cannot. Specifically, joint angle predictions made by the pose map $\mathbf{\Theta}(F_z, X_w)$ trained with Active Learning ensures force normality and follows the normal force profile closely throughout the clamping operation. However, joint angle predictions made by the pose map $\mathbf{\Theta}(F_z, X_w)$ trained with Linear Positioning Learning results in a violation of the force normality as the torque T_y exceeds the acceptable value of -0.3 Nm and F_z diverges from the desired normal force profile.

5.2.3 Learned Robot Pose Map Speeds-up Operations

Active Learning enables high speed operations, which improves process efficacy. If the pose is being learned during the clamping process, then the rate of change of normal force has to be small to ensure that the changes in deformation are small and do not cause excessive shear force and torque before the robot pose is corrected. However, after learning the pose map, the rate of change of normal force can be higher. In particular, using the pose map $\mathbf{\Theta}(F_z, X_w)$ from the Active Learning process and the methods described in Section 5.1.6 it is possible to increase the predicted robot-workpiece-interaction speeds at unmeasured workpiece locations. The increased speeds are accomplished by reducing the time scale of the prescribed sigmoidal normal force profile in Fig. 5.5 which subsequently reduces the time scale of the predicted robot joint angles in Fig. 5.6 by the same amount. The resulting shear forces F_x and torques T_y for predictable interactions at a workpiece location of $X_w = 355$ mm are presented in Fig. 5.8 and Fig. 5.9 respectively. With increasing interaction speeds of 1, 2, 4, and 8 times the original measurement process operating speed of 93 seconds, the shear force F_x remains well within the acceptable range of $|F_x| < 15$ N and the torque Ty

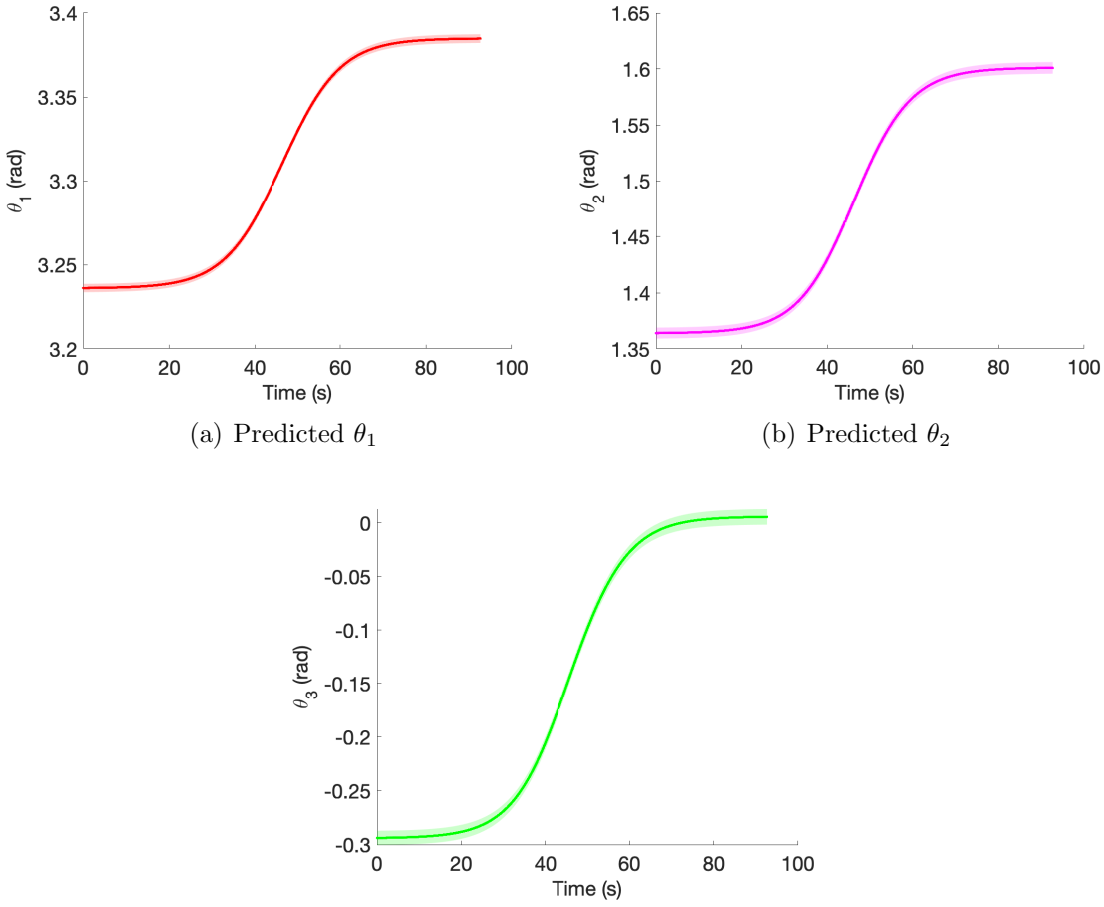

(a) Predicted θ_1

(b) Predicted θ_2

(c) Predicted θ_3

Figure 5.6: Predicted robot joint angles for a robot-workpiece interaction at a location of $X_w = 355$ mm, for the Active Learning process. The solid line in each plot is the predicted value for each joint angle, the shaded area around each line is the standard deviation of each prediction.

approaches the upper limit yet remains within an acceptable range of $|T_y| < 0.3$ Nm. This indicates that force normality with the workpiece is maintained up to 8 times the original interaction speed. The process takes only 11.6 seconds and is a 87.5% reduction in the time needed for the robot-workpiece interaction. Thus, force normality at unmeasured workpiece locations can be ensured and the clamping operation can be sped up by the robot pose map $\boldsymbol{\Theta}(F_z, X_w)$ that is trained with the Active Learning approach.

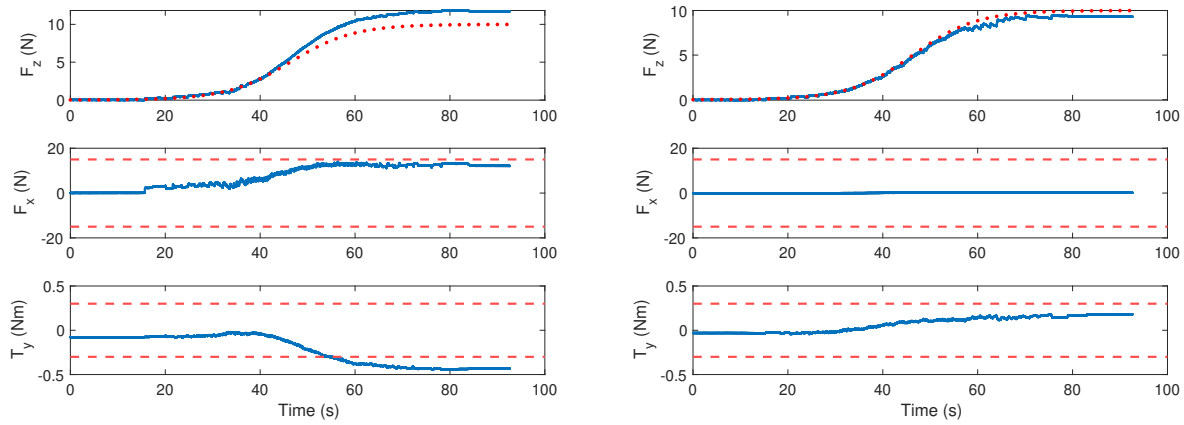

(a) Linear Positioning Learning

(b) Active Learning

Figure 5.7: Measured forces and torque for the GPR predicted interaction at the unmeasured workpiece location of $X_w = 355$ mm. The desired normal force profiles are are shown by the dotted red lines and acceptable force and torque limits are shown by the dashed red lines. (a) The Linear Positioning Learning process can not accurately correct for the robot-beam interaction and maintain force normality, as the torque T_y exceeds the permissible torque limits. (b) The Active Learning process can, however, effectively correct for the robot-beam interaction and maintain force normality without exceeding any of the permissible limits on shear force F_x or torques T_y.

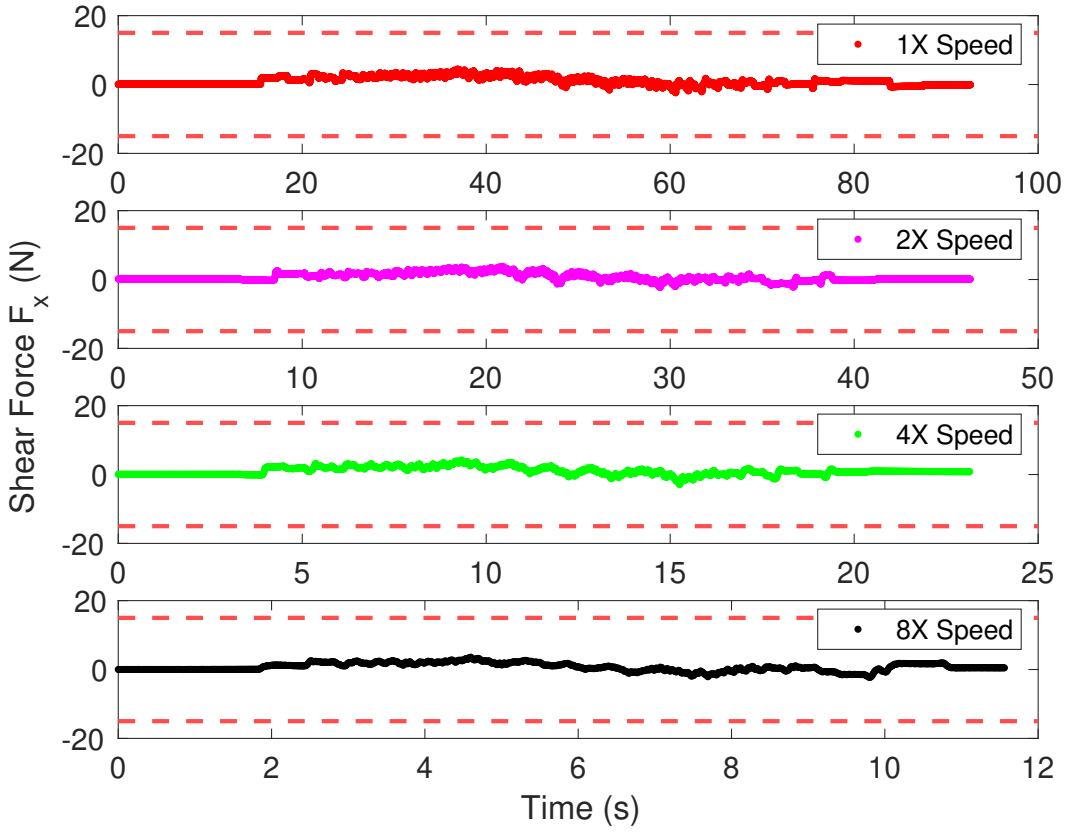

Figure 5.8: Force normality at high operating speeds. Measured shear force F_x, with the Active Learning GPR predicted pose trajectories at the workpiece location $X_w = 355$ mm as the interaction speed is increased, remains within acceptable shear force limits indicated by the dashed red lines.

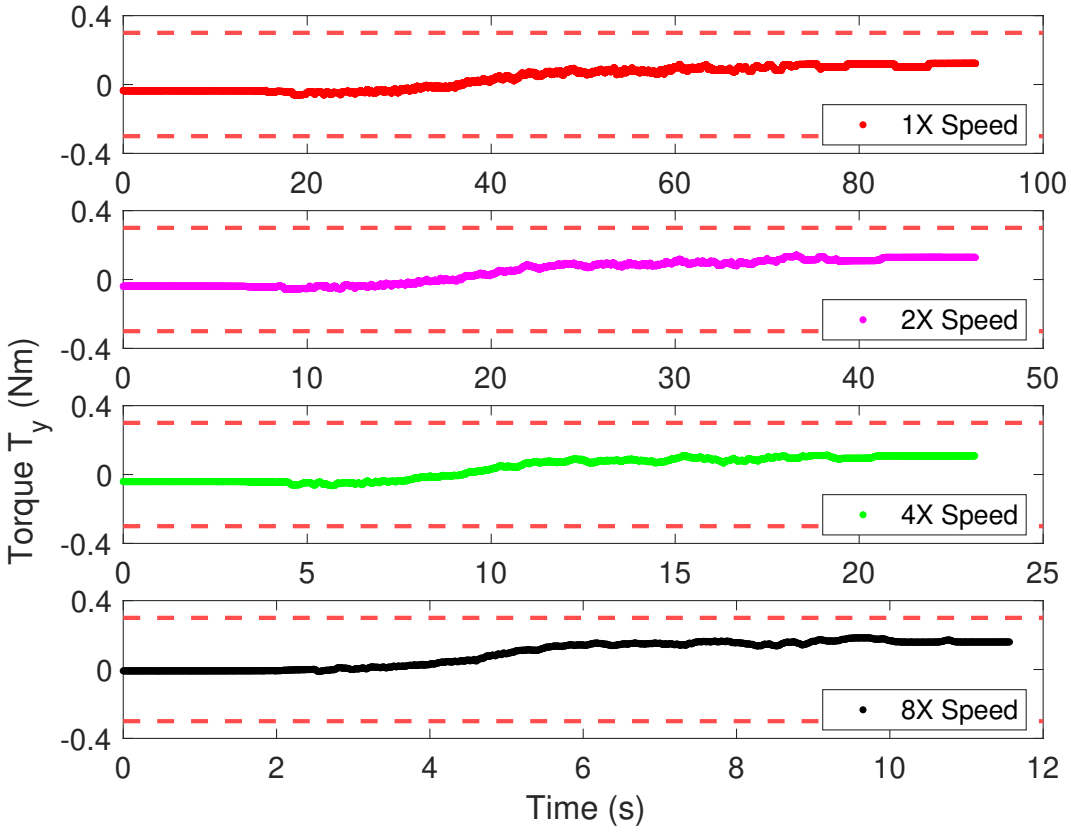

Figure 5.9: Force normality at high operating speeds. Measured torque T_y, with the Active Learning GPR predicted pose trajectories at the workpiece location $X_w = 355$ mm as the interaction speed is increased, remains within acceptable torque limits indicated by the dashed red lines.

5.3 Chapter Conclusions

This study developed and assessed a data-enabled active learning method for the interaction of robots with flexible structures, taking into consideration the elasticity of both the robot and the workpiece. The approach employs Gaussian Process Regression techniques to acquire the robot pose map for achieving a desired normal force at specific unmeasured points on the workpiece while ensuring small shear force and torques (i.e., ensuring normality) between the

tool and workpiece. Experimental results demonstrate that the active learning approach can significantly reduce the required number of measurements to learn the pose map by 77.8%. Additionally, once the pose map is learned, it proves effective in predicting robot-workpiece interactions at unmeasured locations as well as maintaining tool-workpiece normality at eight times the original operating speed.

Chapter 6

SUMMARY AND FUTURE WORK

6.1 Summary

The primary contributions of this thesis are as follows: Firstly, it demonstrates that data collected during robotic clamping operations can be learned and utilized to expedite similar processes. By leveraging the learned parameters, a map between the measured forces and robot joint positions is created to develop time-based robot-joint (velocity) trajectories, ensuring a specified robot-workpiece interaction. Experimental results indicate that the operational speed can be increased while maintaining interaction forces and torques within acceptable limits. Secondly, it shows that with a minimal number of learned measurement locations, controlled interactions, such as clamping operations, can be efficiently predicted at unmeasured locations. Gaussian Process Regression methods are introduced as an effective means to predict interactions, leading to increased interaction speeds at workpiece locations where controlled interactions have not been previously performed. Additionally, to reduce the number of measurement locations, a method is developed using existing interaction data to optimize measurement location selection by minimizing prediction uncertainty.

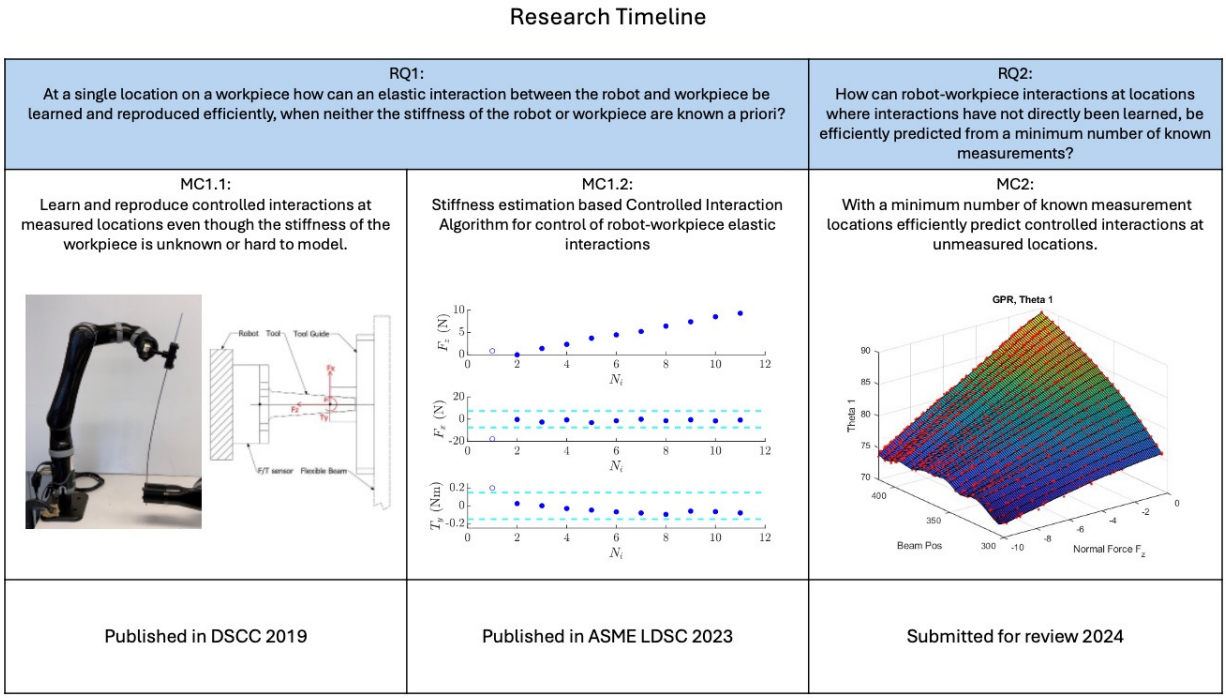

Figure 6.1: Timeline of research with research questions, main contributions and related publications [1, 2, 3].

The main contributions of the dissertation are outlined in Fig. 6.1, with further elaboration on these contributions provided subsequently.

1. Chapter 3 addresses the main contribution **MC1.1**; *Learn and reproduce controlled interactions at measured locations even though the stiffness of the workpiece is unknown or hard to model*, and has been published in [1]. Efficient and accurate robotic interactions with flexible structures are critical for many manufacturing processes where the elasticity of the workpiece and the robot must be accounted for. In particular, for clamping and drilling flexible structures, maintaining tool-workpiece normality and limiting shear forces are essential. The main contribution of this chapter is to show experimentally, that data acquired during a robotic clamping operation can be used to

speed up the process for similar operations. Utilizing the learned parameters, a map between the measured forces and robot joint positions is used to develop time-based robot-joint (velocity) trajectories to achieve a specified robot-workpiece interaction. Experimental results show that the operating speed can be increased by three times while maintaining interaction forces and torques within acceptable levels.

2. Chapter 4 addresses the main contribution **MC1.2**; *Stiffness estimation based Controlled-Interaction Algorithm for control of robot-workpiece elastic interactions*, and has been published in [2]. The challenge is that the combined stiffness of a robot and workpiece, needed to control the robot-workpiece elastic interactions are often difficult to model and can vary due to geometry changes of the workpiece caused by large deformations and associated pose variations of the robot. The main contribution of this chapter is an algorithm, (i) to learn the robot-workpiece stiffness relationship using a model-free data-based approach and (ii) to use it for applying desired forces and torques on the elastic structure. Moreover, comparative experiments with and without the data-based stiffness estimation show that clamping operating speed is increased by four times when using the stiffness estimation method while interaction forces and torques are kept within acceptable bounds.

3. Chapter 5 addresses the main contribution **MC2**; *With a minimum number of known measurement locations efficiently predict controlled interactions at unmeasured locations*, and has been submitted for publication as a journal article [3]. During manufacturing processes, for instance clamping and drilling elastic structures, it's crucial to maintain normality of the tool-workpiece forces for minimizing shear forces and torques to avoid tool or workpiece damage. The difficulty lies in precision model-based predictions of the relatively-large deformations as the applied force is increased, due

to the robot-workpiece elastic interactions, which are needed for selecting the appropriate robot pose that ensures force normality. Therefore, recent works have used force-displacement measurements at each work location to select the robot pose for ensuring tool normality — however, such local-estimation-based approach at each work location can be slow and therefore, time prohibitive. The main contributions of this chapter are: (i) to use Gaussian Process Regression (GPR) methods [24] to learn the robot pose for force normality at unmeasured workpiece locations; and (ii) to use active learning for optimally selecting and minimizing the number of measurement locations needed for accurate learning of the robot-pose map with the data enabled approach. Experimental results show that the number of data points needed with active learning is 77.8% less than the case with a benchmark Linear Positioning learning for the same level of model precision. Moreover, the learned robot-pose map enables rapid increase of the normal force in the presence of elastic interactions at unmeasured locations on the workpiece, reaching speeds up to eight times faster than the original interaction speed when the robot is learning the correct pose.

6.2 Future Work

This section explores possible future work for control and prediction of robot-structure elastic interactions, informed by the findings of this dissertation.

1. The robot-workpiece elastic interactions studied in this dissertation are limited to a planar interaction (requiring a 3 degree of freedom robot) with a workpiece that has smooth stiffness variations. Demonstrating that the methods presented here are generalisable would prove valuable in real world applications. An application such as robotic drilling, requiring a 6 degree of freedom robot where the relative robot-workpiece stiffness changes rapidly as the drill bit exits the workpiece would naturally extend this work as many of the same constraints are required (limiting F_x and T_y, while controlling F_z). Therefore, future research could explore interactions that require a full 6 degree of freedom robot and workpieces that have highly variable stiffness variations.

2. In this dissertation the set of robot-workpiece interaction locations was limited to a discrete set of known locations on the workpiece. However, for many manufacturing operations this may not be the case, a continuous set of possible workpiece locations may be available. For an unexplored set of workpiece locations that cover a continuous space, gradient-based or Bayesian optimization methods, [59], could be used to find the next workpiece location $X_{w,J+1}$ in line 8 of Algorithm 4. Therefore, future research can explore the feasibility of controlling and predicting elastic interactions between robots and structures across a wider range of manufacturing applications.

BIBLIOGRAPHY

[1] Lance McCann, Chia-Ning Lee, Yoshua Gombo, Joseph Garbini, and Santosh Devasia. Data-based learning for control of elastic interactions between robot and workpiece. In *Dynamic Systems and Control Conference*, volume 59148, page V001T10A005. American Society of Mechanical Engineers, 2019.

[2] Lance McCann, Yoshua Gombo, Anuj Tiwari, Joseph Garbini, and Santosh Devasia. Data-based stiffness estimation for control of robot–workpiece elastic interactions. *ASME Letters in Dynamic Systems and Control*, 3(3), 2023.

[3] Lance McCann, Leon (Liangwu) Yan, Sarmad Hassan, Joseph Garbini, and Santosh Devasia. Active data-enabled robot learning of elastic workpiece interactions. *Submitted for publication as a journal article*, 2024.

[4] J. R. Diaz Posada, U. Schneider, S. Pidan, M. Geravand, P. Stelzer, and A. Verl. High accurate robotic drilling with external sensor and compliance model-based compensation. In *2016 IEEE International Conference on Robotics and Automation (ICRA)*, pages 3901–3907, May 2016.

[5] Y. Gao, D. Wu, C. Nan, X. Ma, and K. Chen. Optimization design for normal direction measurement in robotic drilling. *ASME International Mechanical Engineering Congress and Exposition*, (46445):V02BT02A033–, 2014.

[6] WIRED. It takes 60,000 rivets and two robots to build a boeing 777 fuselage. [Video], Dailymotion, https://www.dailymotion.com/video/x5fhvdn, March 2017.

[7] Felix Nadon, Angel J. Valencia, and Pierre Payeur. Multi-modal sensing and robotic manipulation of non-rigid objects: A survey. *Robotics*, 7(4), 2018.

[8] Jose Sanchez, Juan-Antonio Corrales, Belhassen-Chedli Bouzgarrou, and Youcef Mezouar. Robotic manipulation and sensing of deformable objects in domestic and industrial applications: a survey. *The International Journal of Robotics Research*, 37(7):688–716, 2018.

[9] FANUC. Aerospace drilling robot. [Photograph], FANUC America Corporation, https://www.fanucamerica.com/solutions/industries/aerospace, 2017.

[10] CORO LAB. Robotiq gripper and various objects from amazon picking challenge. [Photograph], IEEE Spectrum, https://spectrum.ieee.org/why-tactile-intelligence-is-the-future-of-robotic-grasping, 2015.

[11] Elmira Madadi and Dirk Söffker. Model-free approaches applied to the control of nonlinear systems: A brief survey with special attention to intelligent pid iterative learning control. *ASME Dynamic Systems and Control Conference*, (57243):V001T03A004–, 2015.

[12] T.M. Maupong and P. Rapisarda. Data-driven control: A behavioral approach. *Systems & Control Letters*, 101:37 – 43, 2017. Jan C. Willems Memorial Issue, Volume 2.

[13] P. R. Ouyang and Pong-in Pipatpaibul. Iterative learning control: A comparison study. *ASME International Mechanical Engineering Congress and Exposition*, (44458):939–945, 2010.

[14] Marnix Volckaert, Jan Swevers, and Moritz Diehl. A two step optimization based iterative learning control algorithm. *ASME 2010 Dynamic Systems and Control Conference, Volume 1*, (44175):579–581, 2010.

[15] Shuwen Yu and Masayoshi Tomizuka. Iterative learning control with optimal feedback and feedforward control. *ASME 2010 Dynamic Systems and Control Conference, Volume 1*, (44175):591–598, 2010.

[16] Yin Bu, Wenhe Liao, Wei Tian, Jin Zhang, and Lin Zhang. Stiffness analysis and optimization in robotic drilling application. *Precision Engineering*, 49:388 – 400, 2017.

[17] S. van Duin and H. Kihlman. Robotic normalizing force feedback. In *Aerospace Technology Conference and Exposition*. SAE International, oct 2005.

[18] Yingjie Guo, Huiyue Dong, and Yinglin Ke. Stiffness-oriented posture optimization in robotic machining applications. *Robotics and Computer-Integrated Manufacturing*, 35:69–76, 2015.

[19] Tomas Olsson, Mathias Haage, Henrik Kihlman, Rolf Johansson, Klas Nilsson, Anders Robertsson, Mats Björkman, Robert Isaksson, Gilbert Ossbahr, and Torgny Brogårdh.

[20] Laixi Zhang, Jaspreet Dhupia, and Mingliang Wu. Analysis and comparison of control strategies for normal adjustment of a robotic drilling end-effector. *Journal of Vibroengineering*, 20, 11 2018.

[21] Andreas Frommknecht, Jens Kuehnle, Ira Effenberger, and Sergej Pidan. Multi-sensor measurement system for robotic drilling. *Robotics and Computer-Integrated Manufacturing*, 47:4 – 10, 2017. SI: FAIM 2015.

[22] Zhong-Sheng Hou and Zhuo Wang. From model-based control to data-driven control: Survey, classification and perspective. *Information Sciences*, 235:3 – 35, 2013. Data-based Control, Decision, Scheduling and Fault Diagnostics.

[23] Hui Xiao, Yaakov Bar-Shalom, and Xu Chen. Model-based sparse information recovery by a collaborative sensor management. (51890):V001T01A009–, 2018.

[24] Carl Edward Rasmussen. Gaussian processes in machine learning. In *Summer School on Machine Learning*, pages 63–71. Springer, 2003.

[25] J Kenneth Salisbury. Active stiffness control of a manipulator in cartesian coordinates. In *1980 19th IEEE conference on decision and control including the symposium on adaptive processes*, pages 95–100. IEEE, 1980.

[26] Milos Zefran and Vijay Kumar. Affine connections for the cartesian stiffness matrix. In *Proceedings of international conference on robotics and automation*, volume 2, pages 1376–1381. IEEE, 1997.

[27] Anatol Pashkevich, Alexandr Klimchik, and Damien Chablat. Enhanced stiffness modeling of manipulators with passive joints. *Mechanism and machine theory*, 46(5):662–679, 2011.

[28] Shih-Feng Chen and Imin Kao. Conservative congruence transformation for joint and cartesian stiffness matrices of robotic hands and fingers. *The International Journal of Robotics Research*, 19(9):835–847, 2000.

[29] Shih-Feng Chen and Imin Kao. Geometrical approach to the conservative congruence transformation (cct) for robotic stiffness control. In *Proceedings 2002 IEEE International Conference on Robotics and Automation (Cat. No. 02CH37292)*, volume 1, pages 544–549. IEEE, 2002.

[30] Yanmei Li, Shih-Feng Chen, and Imin Kao. Stiffness control and transformation for robotic systems with coordinate and non-coordinate bases. In *Proceedings 2002 IEEE International Conference on Robotics and Automation (Cat. No. 02CH37292)*, volume 1, pages 550–555. IEEE, 2002.

[31] Shih-Feng Chen. The 6x6 stiffness formulation and transformation of serial manipulators via the cct theory. In *2003 IEEE International Conference on Robotics and Automation (Cat. No. 03CH37422)*, volume 3, pages 4042–4047. IEEE, 2003.

[32] Gürsel Alici and Bijan Shirinzadeh. Enhanced stiffness modeling, identification and characterization for robot manipulators. *IEEE transactions on robotics*, 21(4):554–564, 2005.

[33] Claire Dumas, Stéphane Caro, Mehdi Cherif, Sébastien Garnier, and Benoît Furet. Joint stiffness identification of industrial serial robots. *Robotica*, 30(4):649–659, 2012.

[34] Yin Bu, Wenhe Liao, Wei Tian, Jin Zhang, and Lin Zhang. Stiffness analysis and optimization in robotic drilling application. *Precision Engineering*, 49:388–400, 2017.

[35] Longfei Sun and Lijin Fang. An approximation method for stiffness calculation of robotic arms with hybrid open-and closed-loop kinematic chains. *Advances in Mechanical Engineering*, 10(2):1687814018761297, 2018.

[36] Andrea Cirillo, Pasquale Cirillo, Giuseppe De Maria, Ciro Natale, and Salvatore Pirozzi. Control of linear and rotational slippage based on six-axis force/tactile sensor. In *2017 IEEE International Conference on Robotics and Automation (ICRA)*, pages 1587–1594. IEEE, 2017.

[37] Nima Fazeli, Miquel Oller, Jiajun Wu, Zheng Wu, Joshua B Tenenbaum, and Alberto Rodriguez. See, feel, act: Hierarchical learning for complex manipulation skills with multisensory fusion. *Science Robotics*, 4(26):eaav3123, 2019.

[38] Sergio Caccamo, Püren Güler, Hedvig Kjellström, and Danica Kragic. Active perception and modeling of deformable surfaces using gaussian processes and position-based dynamics. In *2016 IEEE-RAS 16th International Conference on Humanoid Robots (Humanoids)*, pages 530–537. IEEE, 2016.

[39] Alexander Verl, Anna Valente, Shreyes Melkote, Christian Brecher, Erdem Ozturk, and Lutfi Taner Tunc. Robots in machining. *CIRP Annals*, 68(2):799–822, 2019.

[40] MJR Costa, RM Gouveia, FJG Silva, and RDSG Campilho. How to solve quality problems by advanced fully-automated manufacturing systems. *The International Journal of Advanced Manufacturing Technology*, 94:3041–3063, 2018.

[41] Benjamin Pereira, Christian Andrew Griffiths, Benjamin Birch, and Andrew Rees. Optimization of an autonomous robotic drilling system for the machining of aluminum aerospace alloys. *The International Journal of Advanced Manufacturing Technology*, pages 1–16, 2022.

[42] Toni Cvitanic, Vinh Nguyen, and Shreyes N Melkote. Pose optimization in robotic machining using static and dynamic stiffness models. *Robotics and Computer-Integrated Manufacturing*, 66:101992, 2020.

[43] Tomas Olsson, Mathias Haage, Henrik Kihlman, Rolf Johansson, Klas Nilsson, Anders Robertsson, Mats Björkman, Robert Isaksson, Gilbert Ossbahr, and Torgny Brogårdh. Cost-efficient drilling using industrial robots with high-bandwidth force feedback. *Robotics and Computer-Integrated Manufacturing*, 26(1):24–38, 2010.

[44] Andreas Frommknecht, Jens Kuehnle, Ira Effenberger, and Sergej Pidan. Multi-sensor measurement system for robotic drilling. *Robotics and Computer-Integrated Manufacturing*, 47:4–10, 2017.

[45] Zhong-Sheng Hou and Zhuo Wang. From model-based control to data-driven control: Survey, classification and perspective. *Information Sciences*, 235:3–35, 2013.

[46] Wei Ji and Lihui Wang. Industrial robotic machining: a review. *The International Journal of Advanced Manufacturing Technology*, 103:1239–1255, 2019.

[47] Zheng Wang, Runan Zhang, and Patrick Keogh. Real-time laser tracker compensation of robotic drilling and machining. *Journal of Manufacturing and Materials Processing*, 4(3):79, 2020.

[48] Ulrich Schneider, Manuel Drust, Matteo Ansaloni, Christian Lehmann, Marcello Pellicciari, Francesco Leali, Jan Willem Gunnink, and Alexander Verl. Improving robotic machining accuracy through experimental error investigation and modular compensation. *The International Journal of Advanced Manufacturing Technology*, 85:3–15, 2016.

[49] Ikenna Enebuse, Mathias Foo, Babul Salam Ksm Kader Ibrahim, Hafiz Ahmed, Fhon Supmak, and Odongo Steven Eyobu. A comparative review of hand-eye calibration techniques for vision guided robots. *IEEE Access*, 9:113143–113155, 2021.

[50] Jen-Chung Hsiao, Kumar Shivam, I-Fang Lu, and Tai-Yan Kam. Positioning accuracy improvement of industrial robots considering configuration and payload effects via a hybrid calibration approach. *IEEE ACCESS*, 8:228992–229005, 2020.

[51] Ikenna Enebuse, Babul K. S. M. Kader Ibrahim, Mathias Foo, Ranveer S. Matharu, and Hafiz Ahmed. Accuracy evaluation of hand-eye calibration techniques for vision-guided robots. *PLOS ONE*, 17(10), OCT 19 2022.

[52] C. E. Rasmussen and C. K. I. Williams. *Gaussian Processes for Machine Learning*. The MIT Press, Cambridge, MA, 2006.

[53] William S Cleveland and Susan J Devlin. Locally weighted regression: an approach to regression analysis by local fitting. *Journal of the American statistical association*, 83(403):596–610, 1988.

[54] Nur MM Kalimullah, Kaushik Shukla, Amit Shelke, and Anowarul Habib. Stiffness tensor estimation of anisotropic crystal using point contact method and unscented kalman filter. *Ultrasonics*, 131:106939, 2023.

[55] Burr Settles. Active learning literature survey. 2009.

[56] Xianliang Gong and Yulin Pan. Discussion: "Bayesian Optimal Design of Experiments for Inferring the Statistical Expectation of Expensive Black-Box Functions" (Pandita, P., Bilionis, I., and Panchal, J., 2019, ASME J. Mech. Des., 141(10), p. 101404). *Journal of Mechanical Design*, 144(5):055501, 12 2021.

[57] Dongrui Wu. Pool-based sequential active learning for regression. *IEEE transactions on neural networks and learning systems*, 30(5):1348–1359, 2018.

[58] Robert Chin, Alejandro I Maass, Nalika Ulapane, Chris Manzie, Iman Shames, Dragan Nešić, Jonathan E Rowe, and Hayato Nakada. Active learning for linear parameter-varying system identification. *IFAC-PapersOnLine*, 53(2):989–994, 2020.

[59] Bobak Shahriari, Kevin Swersky, Ziyu Wang, Ryan P Adams, and Nando De Freitas. Taking the human out of the loop: A review of bayesian optimization. *Proceedings of the IEEE*, 104(1):148–175, 2015.

[60] Qiang Zhang and Ming-Yong Zhao. Minimum time path planning of robotic manipulator in drilling/spot welding tasks. *Journal of Computational Design and Engineering*, 3(2):132–139, 2016.

[61] Reginald Dewil, İlker Küçükoğlu, Corrinne Luteyn, and Dirk Cattrysse. A critical review of multi-hole drilling path optimization. *Archives of Computational Methods in Engineering*, 26:449–459, 2019.

Appendix A

ALTERED ROBOT-BEAM CONFIGURATION

A.1 Reproduced Interaction with Robot-Beam Configuration Altered by 2.5mm

In the altered robot-beam configuration, the tool-beam contact location is moved 2.5mm closer to the beam mounting point, away from the location where the controlled-interaction took place. The measured normal forces F_z for each reproduced interaction with the altered robot-beam configuration are plotted in Fig. A.1. For this case the measured normal forces are very similar to the original robot-beam configuration as seen in Fig. 3.7 and F_z reaches and maintains a steady state force of $\approx 91\%$ *to* 94% the target $10N$ force.

Interaction torques T_y for the altered configuration reproduced interaction are plotted in Fig. A.2. Once again the measurements are very similar to the original robot-beam configuration as seen in Fig. 3.8, T_y remains well within the acceptable range of $\pm 0.1Nm$ and tool normality with the workpiece is maintained up to $4X$ the original interaction speed.

Shear forces F_x for the altered configuration reproduced interaction are plotted in Fig. A.3. Notably for this case the similarities to the original robot-beam configuration no longer hold. For all of the interaction speeds F_x exceeds the acceptable range of $\pm 4N$ about halfway through each interaction.

For the altered configuration, an accurate controlled-interaction cannot be reproduced, as shear forces become unacceptable at every interaction speed. This result suggests that small geometric changes in the robot-beam interaction have a significant impact on interaction forces between the tool and workpiece in the shear F_x direction. Additionally, in the Altered-configuration the stiffness of the beam in the F_x direction dominates the interaction.

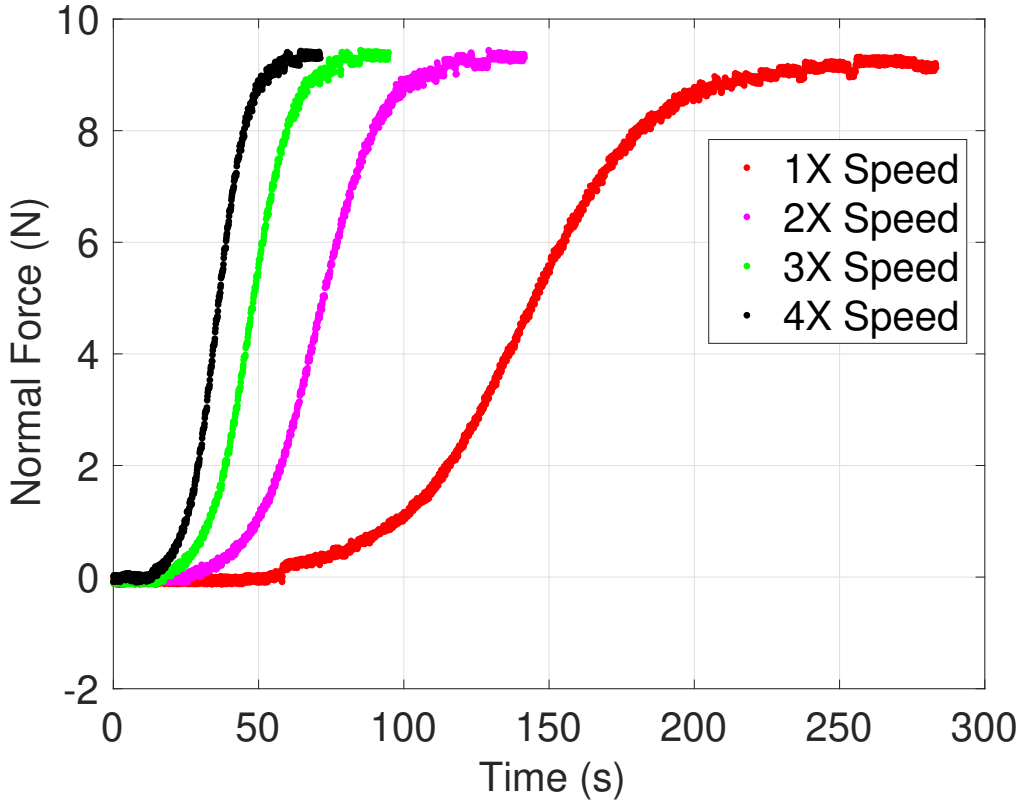

Figure A.1: Measured normal force as speed is increased for the altered robot-beam configuration (tool-beam contact location 2.5mm closer to the beam mounting point).

A.2 CONCLUSIONS

This experimental effort shows that robotic interactions with flexible structures can be learned through data-based methods, however geometrical changes in the robot-workpiece relationship can cause unacceptable errors in a reproduced interaction. The geometrical relationship of the robot and workpiece must be accounted for, even for small changes. If the robot-workpiece contact location is changed, the learned interaction can not be successfully reproduced as large shear forces occur that are beyond acceptable limits. These failures take place at any interaction speed, even the initial learned speed. The failure modes presented

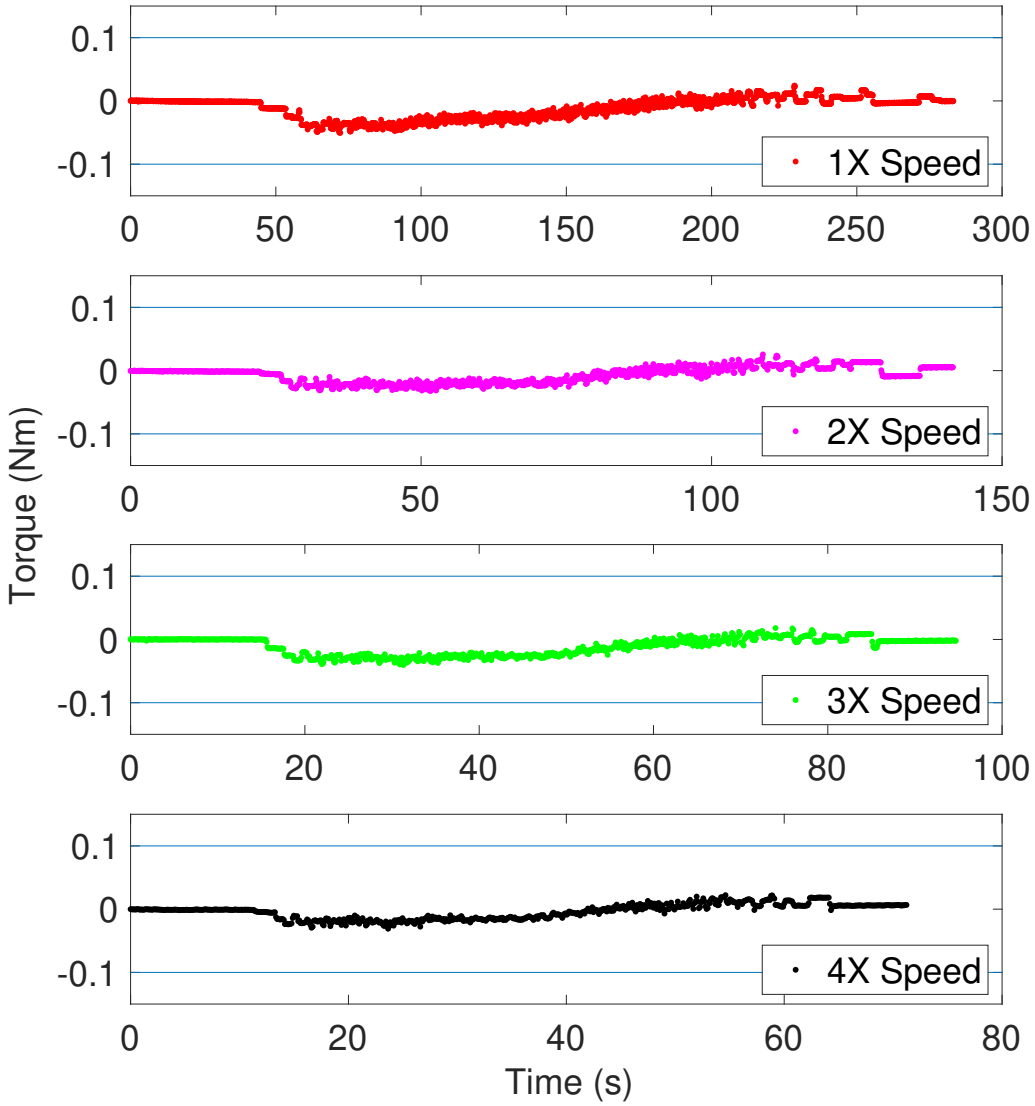

Figure A.2: Measured interaction torque as speed is increased for the altered robot-beam configuration (tool-beam contact location 2.5mm closer to the beam mounting point). Acceptable interaction torque limits are indicated by the blue lines.

here show that the stiffness of the beam dominates the process when the interaction fails in shear. A method that can mitigate excessive shear forces for the altered configuration

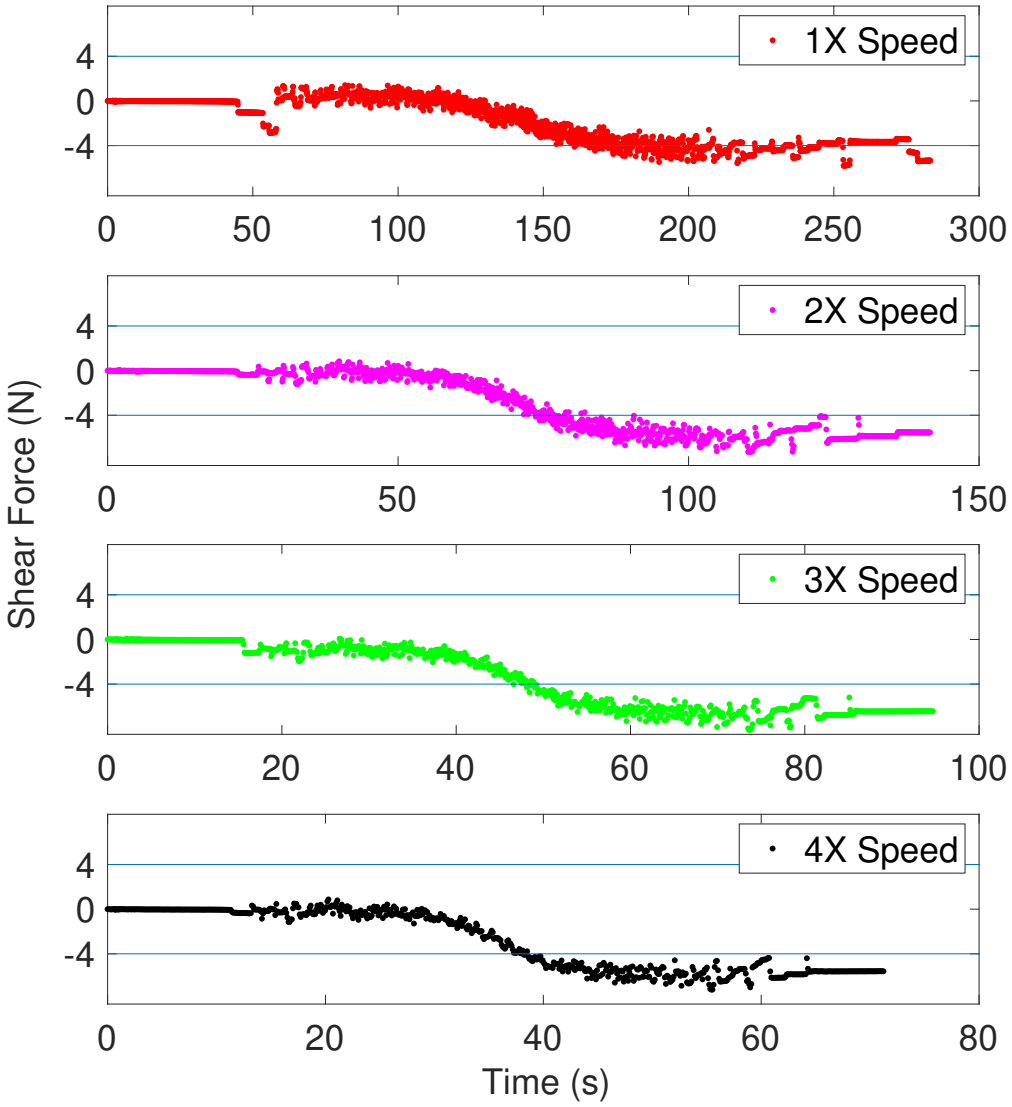

Figure A.3: Measured shear force as speed is increased for the altered robot-beam configuration (tool-beam contact location 2.5mm closer to the beam mounting point). Acceptable shear force limits are indicated by the blue lines.

interaction is required to conduct additional controlled-interactions at a other positions on the beam that have not been learned.

Appendix B

MINIMUM ACHIEVABLE ROBOT JOINT MOVES

The minimum achievable joint motion for each axis of the robot is displayed in Figures B.1, B.2 and B.3. For each robot joint there is a region of approximately ±0.005rad where a commanded motion of the robot will result in effectively no motion of the robot joint.

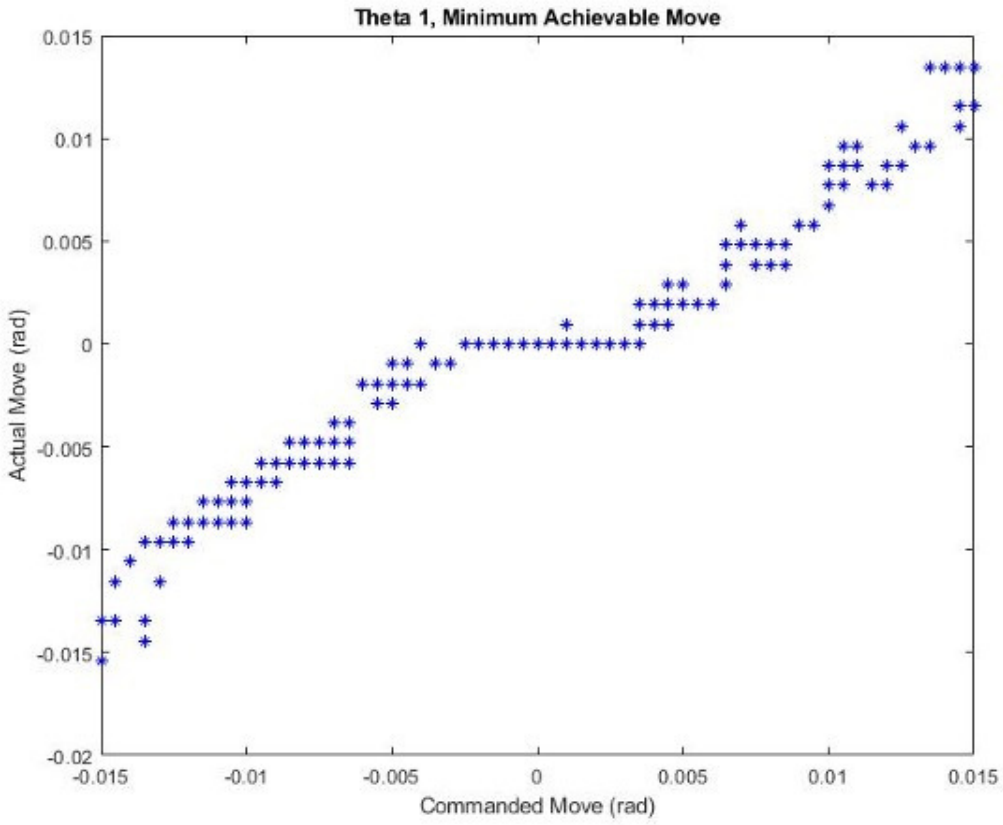

Figure B.1: Minimum achievable robot joint motion for Theta 1.

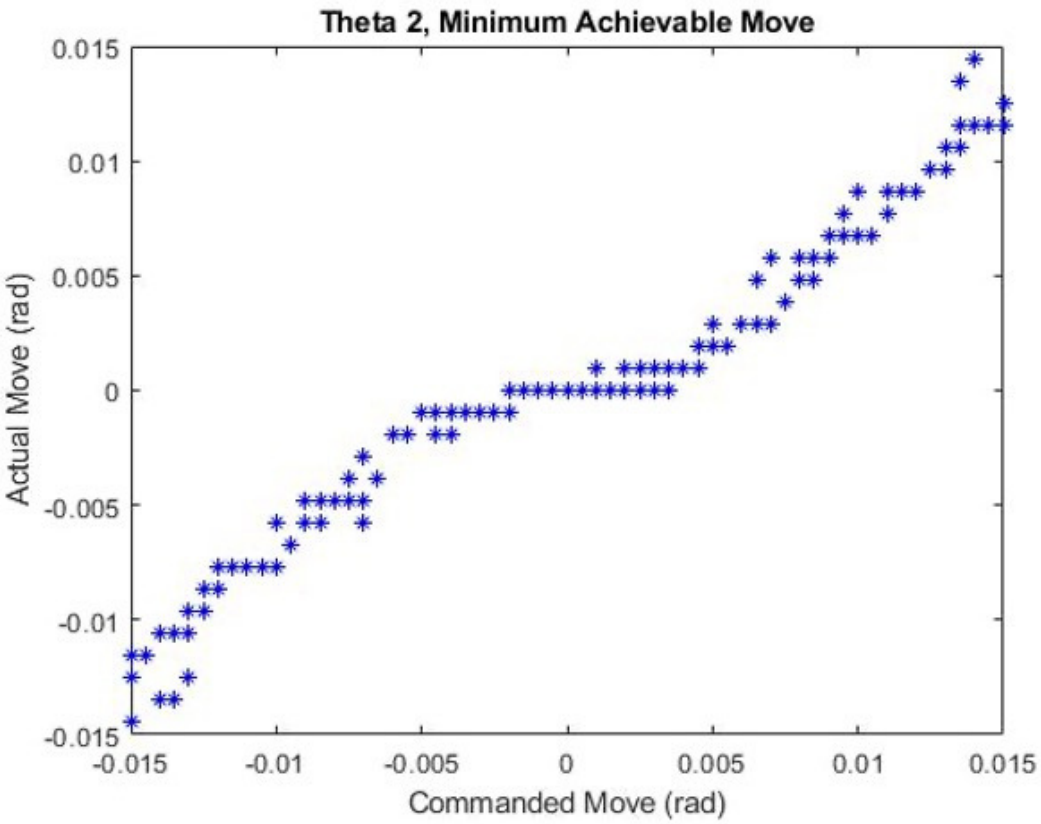

Figure B.2: Minimum achievable robot joint motion for Theta 2.

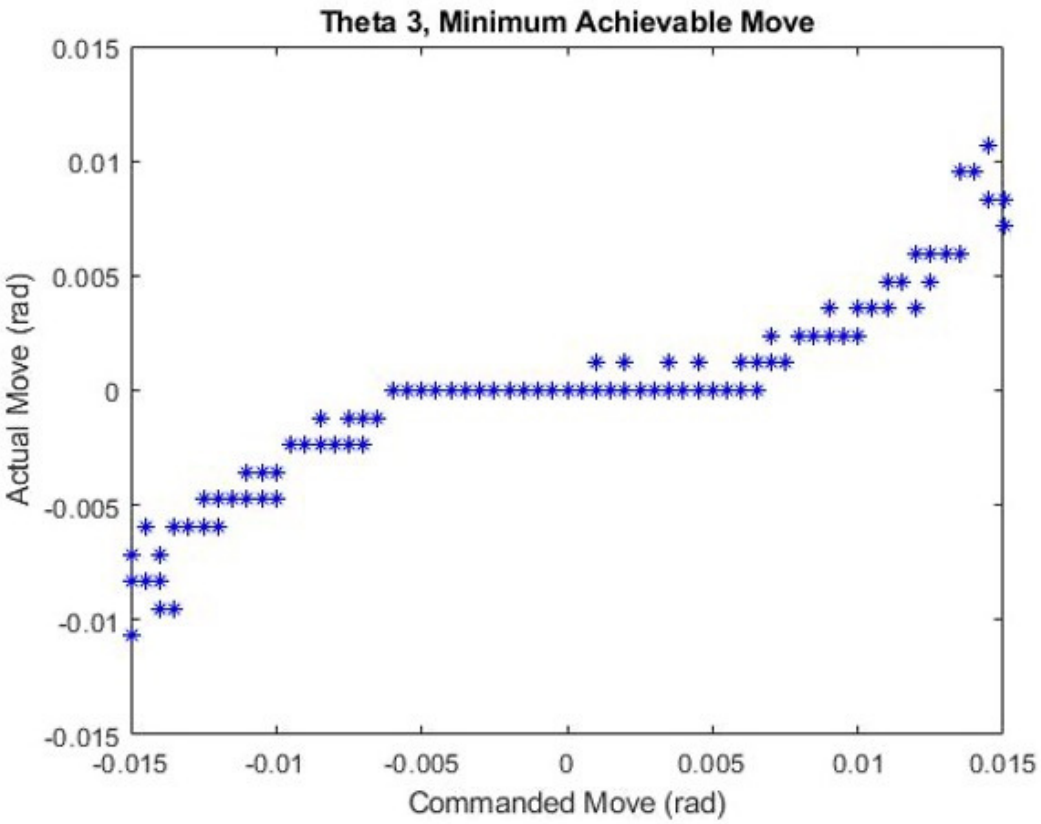

Figure B.3: Minimum achievable robot joint motion for Theta 3.